

AFOSR TR 78-1215

LEVEL II

2

18 AFOSR

UCI

AD A 056746

AD No. DDC FILE COPY

DDC
PROCESSED
JUL 27 1978
E

OPTICAL TRANSMISSION THROUGH THE TURBULENT ATMOSPHERE,

9 FINAL SCIENTIFIC REPORT.

1 Oct 76 - 31 Jan 78

Research Grant AFOSR-76-3097

16 2310

17 A1

15 PRINCIPAL INVESTIGATOR: DR. HIDEYA GAMO

10

11

30 Mar 78

SCHOOL OF ENGINEERING

12 64p.

University of California, Irvine

Irvine, California

406 322

78 07 26 082

Approved for public release; distribution unlimited.

mt

AIR FORCE OFFICE OF SCIENTIFIC RESEARCH (AFSC)
NOTICE OF TRANSMITTAL TO DDC

This technical report has been reviewed and is
approved for public release IAW AFR 190-12 (7b).
Distribution is unlimited.

A. D. BLOSE
Technical Information Officer

REPORT DOCUMENTATION PAGE		READ INSTRUCTIONS BEFORE COMPLETING FORM
1. REPORT NUMBER AFOSR-TR- 78-12	2. GOVT ACCESSION NO.	3. RECIPIENT'S CATALOG NUMBER
4. TITLE (and Subtitle) OPTICAL TRANSMISSION THROUGH THE TURBULENT ATMOSPHERE	5. TYPE OF REPORT & PERIOD COVERED Final Report 1 Oct. 1976-31 Jan. 1978	
	6. PERFORMING ORG. REPORT NUMBER	
7. AUTHOR(s) Hideya Gamo	8. CONTRACT OR GRANT NUMBER(s) AFOSR 76-3097 <i>new</i>	
9. PERFORMING ORGANIZATION NAME AND ADDRESS Univ. of California, Irvine School of Engineering Irvine, California 92717	10. PROGRAM ELEMENT, PROJECT, TASK AREA & WORK UNIT NUMBERS 2310/A1 61102F	
11. CONTROLLING OFFICE NAME AND ADDRESS Air Force Office of Scientific Research/NP Physics Division Bolling Air Force Base, Wash., D.C. 20332	12. REPORT DATE 30 March 1978	
	13. NUMBER OF PAGES 59	
14. MONITORING AGENCY NAME & ADDRESS (if different from Controlling Office)	15. SECURITY CLASS. (of this report) Unclassified	
	15a. DECLASSIFICATION/DOWNGRADING SCHEDULE	
16. DISTRIBUTION STATEMENT (of this Report) Approved for public release, distribution unlimited.		
17. DISTRIBUTION STATEMENT (of the abstract entered in Block 20, if different from Report)		
18. SUPPLEMENTARY NOTES		
19. KEY WORDS (Continue on reverse side if necessary; and identify by block number) C_n^2, strength of turbulence, C_T^2, irradiance fluctuations, temperature structure function, refractive index structure function, laboratory generated turbulence.		
20. ABSTRACT (Continue on reverse side if necessary and identify by block number) A turbulence chamber (0.78 m x 0.23 m x 2.59 m) consisting of 10 small electric heater/blowers with 2 mm aluminum wire meshes can generate the nearly homogeneous isotropic turbulence with the region of 0.5 m x 0.05 m x 2 m. The temperature structure constant, squared $C_n^2 = 52.9 \text{ K}^2 \text{ m}^{-2/3}$ was obtained from the temperature structure function measurements using a differential microthermocouple system. → next page		

Unclassified

SECURITY CLASSIFICATION OF THIS PAGE (When Data Entered)

temperature structure
constant

The refractive index structure constant squared $C_n^2 = 3.00 \times 10^{-11} \text{ m}^{-2/3}$ at the wavelength 632.8 nm was calculated from the C_T^2 at the average temperature 53°C. From the measured power spectrum of temperature fluctuations and the average wind velocity 0.41 m/sec we determined the inner and outer scales of turbulence $\lambda_0 = 5.0 \text{ nm}$ and $L_0 = 6.5 \text{ cm}$, respectively. The measured temperature structures fluctuations satisfy the 2/3 and -5/3 power similarity laws, characteristics of the inertial subrange, respectively.

Power spectra, histograms and cumulants of irradiance fluctuations of collimated laser beams (He-Ne 6328 Å) were measured for folded transmissions by a corner-cube reflector and a plane mirror and the direct transmission. Measurements were performed by using an atmospheric turbulence chamber (one-way path length 1.27 m) and also in the outside field (one way path length 274 meter).

Unclassified

Optical Transmission Through Turbulent Atmosphere

ACCESSION for		
NTIS	White Section	<input checked="" type="checkbox"/>
DDC	Buff Section	<input type="checkbox"/>
UNANNOUNCED		<input type="checkbox"/>
JUSTIFICATION.....		
.....		
DISTRIBUTION/AVAILABILITY CODES		
Dist.	AVAIL.	and/or SPECIAL
A		

FINAL REPORT

Research Grant: AFOSR 76-3097
Period: 1 Oct., 1976 - 31 Jan., 1978
Scientific Monitor: Major William McKechney, AFOSR
Principal Investigator: Dr. Hideya GAMO

Professor of Electrical Engineering
University of California, Irvine
School of Engineering
Irvine, California 92717

78 07 26 082

OPTICAL TRANSMISSION THROUGH THE TURBULENT ATMOSPHERE

Table of Contents

1. Review of Accomplishments 1
2. List of Publications 4
3. Appendix 1: An Atmospheric Turbulence Chamber for..... 6
Optical Transmission Experiment
4. Appendix 2: Comparison of a Corner-Cube Retroreflector... 43
and a Plane Mirror in Folded Path and
Direct Transmission Through Atmospheric
Turbulence

1. REVIEW OF ACCOMPLISHMENTS 1976 - 1978

The highlights of accomplishments during the period are the construction and characterization of the turbulence chamber for optical transmission, and its application to the comparison of optical transmission using a corner-cube, plane mirror and direct transmission. With the objective of clarifying the theoretical models of optical transmission through the turbulent atmosphere, we have built a turbulence chamber and confirmed its isotropic and homogeneous nature of turbulence as well as its C_T^2 and C_n^2 , inner and outer scales of turbulence ℓ_0 and L_0 . Since the strength of this laboratory generated turbulence $C_n^2 = 3 \times 10^{-11} \text{ m}^{-2/3}$ is about 1,000 times larger than that of a typical real atmosphere, it enables us to simulate the essential features of optical transmission under the well-controlled condition. The turbulence thus generated is shown to be locally isotropic and homogeneous within the region where optical transmission experiments were performed. The Kolmogorov-Obukhov 2/3 power law for the temperature structure function was shown to be valid within the localized region of 6 cm diameter. Its details are described in Appendix 1.

The power spectrum of temperature fluctuations in the turbulence chamber closely followed theoretically predicted -5/3 power law for inertial sub-range. From the power spectrum measured, we obtained inner and outer scales of turbulence (ℓ_0 and L , respectively), using G. I. Taylor's hypothesis

of frozen turbulence: $l_0 = 5$ mm and $L_0 = 6.5$ cm.

It was possible with the turbulence chamber to study the optical transmission through turbulence for both regions with Fresnel-zone size smaller and larger than the inner scale of turbulence. We have thus been able to verify some of the theoretical predictions of irradiance fluctuations for both regions. The power spectrum of irradiance fluctuations follow $-8/3$ power on frequency in close agreement with the theory. Details are described in the manuscript to be submitted to Applied Optics. (Publication #2)

By increasing the optical path length through the turbulence chamber, we could reach the so-called saturation region of irradiance fluctuations. The coefficient of variation γ_0 of irradiance fluctuations becomes 1.6, which is close to the observed value in the typical long path propagation in real atmosphere under strong wind conditions. These results will be described in the manuscript to be submitted to Radio Science. (Publication #3)

Comparison of a corner-cube retroreflector and a plane mirror in irradiance fluctuation of the transmission through the turbulence has indicated that the path of propagation for the plane mirror is statistically more independent, whereas for the corner-cube the transmission paths are somewhat correlated. The power spectrums of irradiance fluctuations tend to be wider for the plane mirror case than the corner-cube case. This can be explained qualitatively consi-

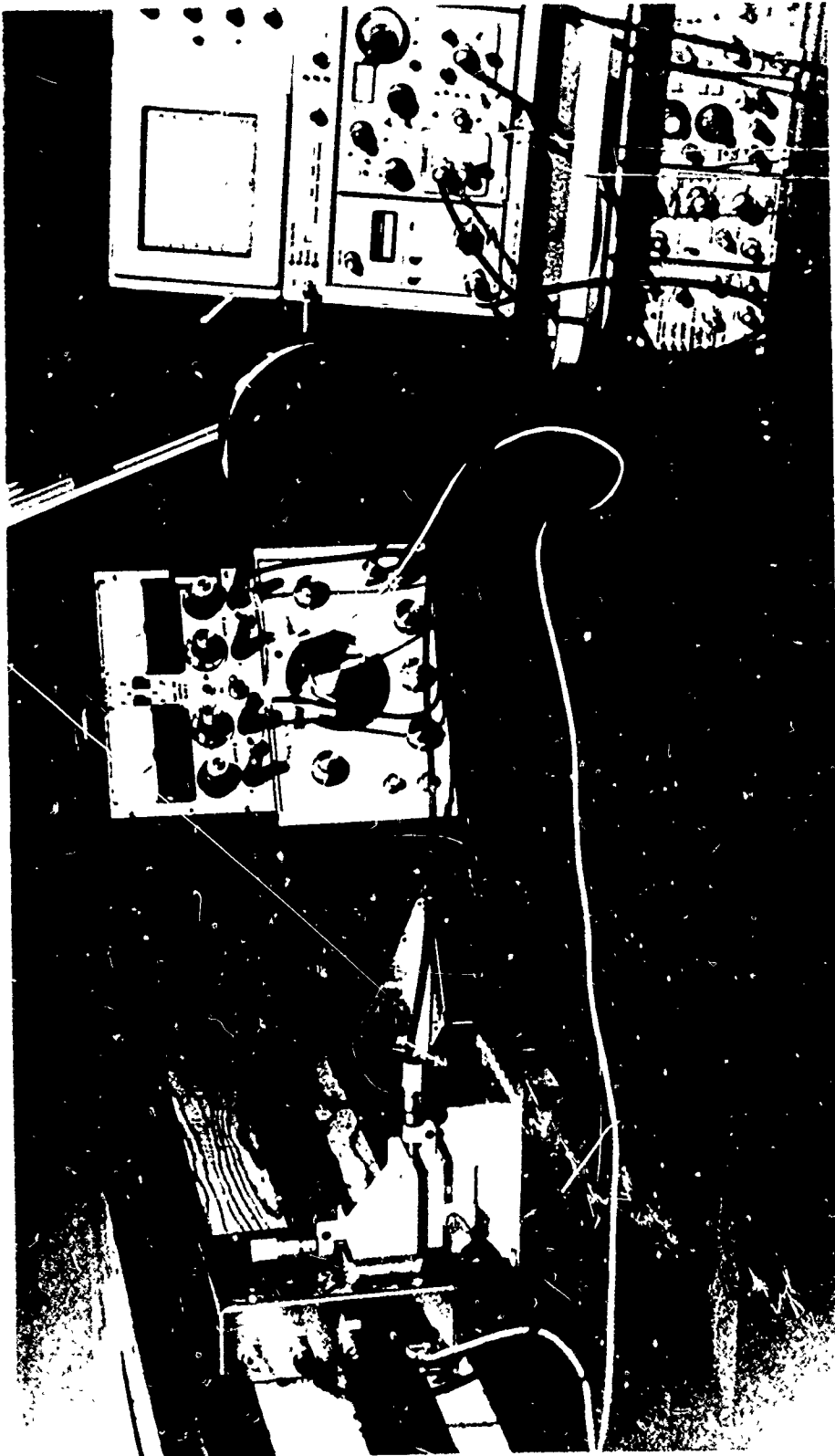
dering the Doppler shift of the scattered light by the turbulence. The reflected beam at corner-cube has components opposite to that of incident with respect to the transverse air flow. Thus, the laser beam of frequency up-shifted by the Doppler effect will suffer the down-shift on the way back. On the other hand, the beam reflected by a plane mirror will produce doppler shift in the same direction as the incident beam. This is described in Appendix II.

Single-ended irradiance fluctuations measurement using a corner-cube retroreflector is convenient from a practical standpoint; scientists at both Naval Ocean Center and National Weather Service have approached us to provide further information on this experiment.

We have performed preliminary experiments of intensity correlation experiments using the 64 diode array interfaced to PDP 15/20 data acquisition system. (See Photograph on Page 6.) This may become a useful tool for measuring the angle of arrival fluctuations and also for characterizing the saturation region in which the multiple scatterin effect becomes significant.

PUBLICATION

1. H. Gamo and A. K. Majumdar, "An Atmospheric Turbulence Chamber for Optical Transmission Experiment: Characterization by Thermal Method," This manuscript has been submitted to Applied Optics.
2. A. K. Majumdar and H. Gamo, "Characterization of an Atmospheric Turbulence Chamber by Laser Irradiance Fluctuation Measurements," This manuscript is to be submitted to Applied Optics.
3. A. K. Majumdar and H. Gamo, "Irradiance Fluctuations of a Laser Beam Under the Multipass Transmission in an Atmospheric Turbulence Chamber," To be submitted to Radio Science.
4. H. Gamo, N. Jagannathan, and A. K. Majumdar, "Comparison of a Corner-Cube Reflector and a Plane Mirror in Folded Path Transmission Through Atmospheric Turbulence," Proc. of the SPIE National Seminar on Advances in Laser Technology for the Atmospheric Sciences, August 25-26, 1977, San Diego, CA, Vol. 125, 1977.



INTENSITY CORRELATION EXPERIMENTS USING
RETICON LINEAR IMAGE SENSORS

APPENDIX I

AN ATMOSPHERIC TURBULENCE CHAMBER FOR OPTICAL TRANSMISSION

EXPERIMENT: CHARACTERIZATION OF THERMAL METHOD*†

Introduction

Artificially generated atmospheric turbulences have been utilized in a few optical propagation and imaging experiments. Most of them, however, were performed without thoroughly specifying the strength of turbulence.¹⁻⁵ We have designed and built a simple atmospheric turbulence chamber with the intention of performing optical wave propagation experiments through the well-defined, homogeneous and isotropic turbulence. Since the refractive index fluctuations in the atmosphere are mainly dependent on the temperature fluctuations,⁶ we utilized the heater/blowers for generating the stronger refractive index fluctuations and made the turbulence more homogeneous and isotropic by passing through metallic screens with random foils and 2 mm screens. In this paper, we shall characterize the atmospheric turbulence in the chamber by the temperature structure constant C_T^2 , which is determined from temperature fluctuation measurements, and then derive the refractive index structure constant C_n^2 from C_T^2 . The C_T^2 of the turbulence chamber was found to be 1,000 times stronger than that of the typical atmosphere. The characterization by the irradiance fluctuation measurements will be described in the second paper.

The histogram, variance and power spectrum of fluctuations of the temperature difference between two micro-thermocouple probes were obtained. The experimental data was processed using a PDP 15/20 system. The temperature structure function (the

mean square temperature difference between two probes) was measured as a function of the probe separation. It is shown that the temperature structure function depends on the $2/3$ power of the probe separation from 2 to 6 cm in accordance with the Kolmogorov-Obukhov similarity law. The temperature structure constants C_T were obtained from these measurements of temperature structure function.⁸

The power spectrum of temperature fluctuations measured inside the turbulence chamber is dependent on the $-5/3$ power of the frequency within the frequency range from 5 to 80 Hz. This agrees with the well-known $f^{-5/3}$ law for the inertial sub-range of homogeneous, isotropic turbulence.^{9,10} By assuming that turbulence eddies were "frozen" while flowing at the mean velocity 0.41 m/sec, we estimated the inner and outer scales of turbulence of the upper and lower frequency limits mentioned above: $\lambda_0=5$ mm and $L_0=8.2$ cm, respectively.

The refractive index structure constants C_n were derived from the temperature structure constants C_T by using the temperature dependence of the refractive index of the atmosphere. The C_n^2 of our turbulence chamber is 1,000 times larger than that of typical turbulence atmosphere.

Different methods for generating the homogeneous isotropic turbulence are compared to our method. Possible improvements of our turbulence chamber and some meaningful aerodynamic experiments are discussed.

The measurement of frequency response function of micro-thermocouples is described in Appendix A and the rms temperature gradient and characteristic temperature of the turbulent temperature field were evaluated by using experimental results and is described in Appendix B.

Design of a Turbulence Chamber

The design of the turbulence chamber is schematically illustrated in Fig. 1. The turbulence chamber with internal dimensions, 2.69 m long, 0.78 m wide and 0.23 m high, was assembled on a shock-mounted optical bench. The internal surface of side-walls, top covers and aluminum plates of the optical bench were coated by a special black paint (3M 101 CID) in order to minimize disturbances due to the reflection of the scattered light by the chamber walls.

Ten small electric heater/blowers (Sears, 764, H, Model 344) were installed on the one side of the turbulence chamber. The turbulent flows generated by the heater/blowers are parallel to the optical bench surface and perpendicular to the optical transmission direction. The height of the center of the flow was almost equal to our standard height for optical measurements, 0.11 m. The turbulent flow generated by the heater/blowers was homogenized by passing through a screen of aluminum foil (commonly used in electronic instruments for ventilation filters) and then through three layers of 2 mm square aluminum meshes, each of which is separated by 1 cm. The turbulent flow produced by heater/blowers operated at the rate of 750 watts was found convenient for the various optical transmission experiments, because of its large strength of turbulence.

Average Wind Velocity and Temperature Distribution

The wind velocity and temperature were measured along the flow direction (x) by a hot wire anemometer (Alnor Thermo-Anemometer 8500) throughout the turbulence chamber at the standard height 0.11 m. The results of wind velocity measurements are shown in Fig. 2. The uniformity of the wind velocity in the flow direction (x) improved with distance from the last screen. At $x=0.61$ m, the wind velocity became fully uniform. The average wind velocity in the range 0.30 m to 0.61 m was 0.41 m/sec at the standard height of 0.1103 m.

The temperature profile for the case in which the heater/blower was set to 750 watts is shown in Fig. 3. The temperature averaged over the chamber was 53° C. Comparing the results in Figs. 2 and 3, we notice that the temperature distribution became uniform at a much faster rate than the wind velocity distribution.

The development of turbulent flow inside the chamber may be explained in the following way.¹¹ A flow generated by each heater/blower at the inlet of the chamber forms boundary layers on both upper and lower walls, owing to the viscous friction. As flow propagates along the x direction, the interaction between flow shear and inlet turbulence increases. Thus, the thickness of boundary layers formed on both walls will increase in the downstream. As a result, the uniformity of the bulk flow in the y direction will improve. This is exhibited by Fig. 4, where wind velocity profiles along the y axis (height) for $x = 0.013$ m, 0.30 m and 0.61 m from the last screen at the

distance $z=1.09$ m are illustrated. It was concluded that a region in the chamber of about 0.31 m wide (x), 0.076 m high (y) and 2.54 m long (z) has relatively uniform velocity and temperature.

The Reynolds number $Re=ud/\nu$ for the region of uniform flow in the turbulence chamber is $Re=6287$, where the average flow velocity $u=0.41$ m/sec, distance between walls $d=0.23$ m and the kinematic viscosity of air, $\nu=1.5 \times 10^{-5}$ m/sec² are used. According to the standard reference books by Schlichting¹¹ and Vennard and Street,¹² the critical Reynolds numbers for flow between parallel walls are 2740 and 1000, respectively. Since the Reynolds number 6287 calculated for our turbulence chamber is much greater than these critical numbers, the turbulent flow within this region of the chamber should be locally homogeneous and isotropic.¹³ This is well-evidenced by the experimental results described in the next section.

Measurements of Temperature Structure Functions

The temperature structure function $D_T(r)$ is defined⁶ as the mean square of the temperature difference between two points, r_1 and r_2 :

$$D_T(r_1, r_2) = \langle [T(r_1) - T(r_2)]^2 \rangle . \quad (1)$$

When the temperature field is homogeneous and isotropic, the structure function depends only on the distance between two points $r = |r_1 - r_2|$:

$$D_T(r_1, r_2) = D_T(r) \quad (2)$$

The experimental set-up for the temperature structure function measurement is illustrated in Fig. 5. The distance r between two micro-thermocouple probes mounted on an electro-mechanical translating unit can be adjusted from 2 mm up to 20 cm by the increment of 10 μ m. The mechanical translation unit was driven by an electrical stepping motor (SLO-SYN SS50-1009, Superior Electric Co.) with an external controller, which can be triggered by the pulse from the PDP 15/20 data acquisition system through a digital-to-analog convertor. This electro-mechanical translation unit was placed on the top cover of the turbulence chamber. Only the thermocouple probes supported by the vertical stainless steel tubes were exposed to the turbulent flow (See Fig. 1). The thermocouple probes project horizontally up-stream by 8.5 cm from the

vertical supporting tubes. The temperature fluctuations in the turbulent air flow were measured by using differential micro-thermocouples of chromel-constantan (Type E, Hy-Cal Engineering), of which the diameter is 7.6 μm and the specified time constant is less than 0.1 m/sec. The temperature voltage conversion factor K of the micro-thermocouples was calibrated by using two electric ovens while keeping the temperature of one junction at 53° C and varying the temperature of the other oven: $K = 0.07184 \times 10^{-3}$ volt/°K.

The frequency response of micro-thermocouples is constant from DC to 200 Hz and then decreases to $\frac{1}{2}$ of the DC level at 770 Hz (See Appendix A). Therefore, the micro-thermocouple system can accurately measure the temperature fluctuations of the turbulent atmosphere, of which the predominant frequency component is limited within 200 Hz.

The output voltages of two thermocouples were amplified by differential amplifiers (Tektronix AM 502), respectively, and two single-ended outputs from these amplifiers were connected to the differential input connectors of the third Tektronix amplifier (AM 502) through two 50 Ω coaxial cables of equal length. The temperature difference at two points can be derived from the differential voltage v_o measured by using the formula

$$T_1 - T_2 = \frac{K}{G_1 G_2 G_3} v_o, \quad (3)$$

where K the thermocouple constant, G_1 , G_2 and G_3 are the

gains of three amplifiers mentioned above, v_o is the voltage measured by an analog-to-digital convertor. By inserting Eq. 3 into Eq. 1, we obtain the temperature structure function expressed in terms of quantities measured and calibrated as follows:

$$\langle (T_1 - T_2)^2 \rangle = \frac{K^2}{(G_1 G_2 G_3)^2} \langle v_o^2 \rangle, \quad (4)$$

where the variance $\langle v_o^2 \rangle$ of the output voltage from the third amplifier was determined from the digitized output voltages by the statistical data acquisition system illustrated in Fig. 6.

In the so-called inertial sub-range of the homogeneous isotropic turbulence, the temperature structure function will depend on the 2/3 power of distance r between two probes:⁶

$$D_T(r) = C_T^2 r^{2/3}, \quad (5)$$

where the distance between probes should be much larger than the inner scale of turbulence ℓ_o but much smaller than the outer scale of turbulence L_o : $\ell_o \ll r \ll L_o$, and C_T is the temperature structure constant. This 2/3 power equation is often called the Kolmogorov-Obukhov similarity law.

The temperature structure functions at a location $x = 0.38$ m, $y = 0.12$ m and $z = 1.09$ m, in the turbulence chamber, measured as a function of the probe separation r , are illustrated in the logarithmic scales in Fig. 7. By inspecting these results, we notice that for the probe separation r between 2 and 6 cm, the 2/3 law holds reasonably well. The data points for the

distance r smaller than 2 cm deviate from the 2/3 line. However, the experimental results do not agree with the theoretical temperature structure function for distance within the inner scale of turbulence: $D_T(r) \propto r^2$. This discrepancy is most likely due to the disturbance produced by stems holding a micro-thermocouple. The structure function measured starts to deviate from the 2/3 law at the probe distance $r = 6$ cm and attains a constant value for $r = 7$ cm and higher. This can be explained by considering that for a large probe separation larger than the outer scale of turbulence, the temperature fluctuations at the two probes are uncorrelated. Since the cross term of temperatures in expansion of $\langle (T_1 - T_2)^2 \rangle$ vanish, temperature structure function, $D_T(r)$ becomes independent of r . Furthermore, the measured $D_T(r)$ indicates that the outer scale of turbulence is of the order of 7 cm and the temperature field in this turbulence chamber is locally homogeneous and isotropic within the 6 cm diameter at the standard height.

Using the $\log D_T(r)$ extrapolated by the 2/3 line at $r = 1$ in Fig. 7, we obtain the strength of temperature fluctuations $C_T^2 = 52.9 \text{ }^\circ\text{K}^2 \text{ m}^{-2/3}$. From the measured C_T^2 we also derived the rms temperature gradient $1.898 \text{ }^\circ\text{K/cm}$ and the characteristic temperature $0.949 \text{ }^\circ\text{K}$ (See appendix B).

The uniformity of the strength of turbulence within the chamber was evaluated by performing a series of measurements of mean square temperature difference at a probe separation 2.89 cm where the 2/3 law approximately holds. From the

measured variances of temperature difference fluctuations, we obtained the C_T^2 defined above. The measured C_T^2 are shown in Fig 8. It should be noted that C_T^2 has a maximum value down the turbulent flow from the last screen while both the average velocity and temperature distributions will monotonically decrease. This implies that the mean square temperature gradient takes the maximum value somewhat down the flow around $x = 0.46$ m (refer to Eqs. (A3) and (A4)).

The turbulence strength parameter of temperature fluctuations C_T^2 is small near the inlet of the chamber (i.e., just near the screens adjacent to the heater/blowers.) This indicates that the temperature fluctuations of grid-generated turbulence is small. As the heat flows along x direction, the small eddies interact with eddies generated in the shear layer adjacent to constant temperature walls. As eddies from both sources mix, temperature fluctuations increase. In the region between $x = 0.30$ m and $x = 0.61$ m, the interaction between the two sources of eddies becomes the largest. In the further downstream, the effects of wall temperature become dominant and the net temperature fluctuations decrease.

Power Spectrum of Temperature Fluctuations

By calculating the time average of absolute value squared of Fourier transform of digitized thermocouple output voltage, we estimated the power spectrum of temperature fluctuations. 512 digital samples with sampling interval 1 m sec were processed by the Fast Fourier Transform (FFT) method and were averaged over 20 results. The power spectrum of temperature fluctuations at the location $x = 0.38$, $y = 0.11$ m, $z = 1.09$ m and the probe distance $r = 2.89$ cm are illustrated in Fig. 9. Over the frequency region from $f = 10$ Hz to 30 Hz, the estimated power spectrum $W(f)$ is proportional to $f^{-5/3}$. At the frequency higher than 30 Hz, the power spectrum approximately follows the f^{-7} law, which was obtained by W. Heisenberg⁹ in the viscous dissipation region. At the frequency region below 10 Hz, it approaches a constant value in a manner similar to the atmospheric turbulence model discussed by Strohbehn.¹⁴

In order to determine the transition frequency from the inertial sub-range to the viscous dissipation range, we also calculated $f^2 W(f)$ and showed in Fig. 9. The upper and lower crossing points of the $f^{-5/3}$ line for inertial sub-range with the f^{-7} and constant lines in Fig. 9 are given by $f_h = 80$ Hz and $f_l = 5$ Hz, respectively. Since the inner scale of turbulence equal to λ_0 of the inertial sub-range is given by $\lambda_0 = \nu/f_h$, by inserting the average wind velocity $\nu = 0.406$ m sec and $f_h = 80$ Hz, we obtain $\lambda_0 = 5$ mm. Likewise, by inserting the same average wind velocity and $f_l = 5$ Hz into the outer scale of turbulence $L_0 = \nu/f_l$, we obtain the outer scale of turbulence $L_0 = 8$ cm. The Reynolds numbers for these scales of turbulence $Re^\lambda = \nu \lambda_0 / \nu$ and $Re^L = \nu L_0 / \nu$ are given by $Re^\lambda = 135$ and $Re^L = 2, 165$, respectively.

Statistics of Temperature Fluctuations

The 512 channel histogram of temperature difference at $r = 2$ cm were obtained by using the PDP 15/20 data acquisition system for various locations of the turbulence chamber. From these histograms, we derived the central moments μ_m and cumulants χ_n up to the eighth order.^{15,16} The coefficients of variation γ_0 , skewness γ_1 and excess γ_2 are calculated from measured moments and cumulants, including their error estimates:

$$\gamma_0 = \sigma/\mu_1, \quad (6)$$

$$\gamma_1 = \mu_3/\sigma^3, \quad (7)$$

and

$$\gamma_2 = \mu_4/\sigma^4 - 3, \quad (8)$$

where σ is the standard deviation and σ^2 is the variance. The smoothed frequency distribution curves of temperature can be obtained by inserting the above coefficients into the Edgeworth series:¹⁵

$$f(\xi) = \phi(\xi) - \frac{1}{3!} \gamma_1 \phi^{(3)}(\xi) + \frac{1}{4!} \gamma_2 \phi^{(4)}(\xi) + \frac{10}{6!} \gamma_1^2 \phi^{(6)}(\xi) + \dots, \quad (9)$$

where

$$\phi(\xi) = \frac{1}{\sqrt{2\pi}} \exp\left(-\frac{\xi^2}{2}\right), \quad (10)$$

and

$\phi^{(n)}(\xi)$ is the n-th derivative of $\phi(\xi)$;

$$\phi^{(n)}(\xi) = (-1)^n H_n(\xi) \phi(\xi), \quad (11)$$

and

$$\xi = (x - \mu_1) / \sigma \quad . \quad (12)$$

$H_n(\xi)$ is the Hermite polynomial of degree n :

$$H_0(x) = 1, \quad H_1(x) = x, \quad H_2(x) = x^2 - 1$$

$$H_3(x) = x^3 - 3x, \quad H_4(x) = x^4 - 6x^2 + 3 \quad . \quad (13)$$

The smoothed frequency distribution curves for a few locations along the air flow are shown in Fig. 10. The coefficients of variation, skewness and excess are shown as a function of x in Fig. 11.

According to these results, the frequency distribution of temperature fluctuations near the screens is very close to the gaussian distribution. Generally, in the gaussian random process, the different frequency spectral components are statistically independent. However, when the different frequency components are not independent of each other, statistical distributions become non-gaussian. In the turbulent flow of inertial sub-range, lower frequency spectral components will transfer energy into the higher frequency components. Hence, the histograms of temperature fluctuations in the turbulent flow are generally non-gaussian. In the region of maximum coefficient of variation, $x = 0.46$ m, the wide range of frequency spectral components representing various sizes of eddies should be interacting most actively. According to Fig. 11, the excess coefficients increase along the flow and becomes maximum at $x = 0.54$ m. However, the coefficients of skewness increase monotonically with distance.

Derivation of C_n from C_T

The refractive index fluctuations of the homogeneously turbulent atmosphere at optical wavelength are mainly due to the temperature fluctuations. The refractive index structure function $D_n(r) = \langle [n(r_1) - n(r_2)]^2 \rangle$ in the inertial sub-range can be expressed in the same 2/3 law as the temperature structure function:

$$D_n(r) = C_n^2 r^{2/3}. \quad (14)$$

The refractive index structure constant C_n can be expressed in terms of the temperature structure constant C_T by using the equation of refractive index as a function of temperature and pressure with wavelength as a parameter. The refractive index of the air at the temperature $T^\circ\text{K}$, the pressure p mb and the wavelength λ μm can be approximated by the following formula:¹⁷

$$n - 1 = \frac{77.6 P}{T} \left[1 + \frac{0.00753}{\lambda^2} \right] \times 10^{-6}. \quad (15)$$

Since the refractive index under the constant pressure depends only on the temperature, we obtain:¹⁸

$$C_n = \frac{77.6 P}{T^2} \left[1 + \frac{0.00753}{\lambda^2} \right] \times 10^{-6} C_T. \quad (16)$$

For the normal atmospheric pressure $p = 1,013.25$ mb and the wavelength $\lambda = 0.6328$ μm and the average temperature of the turbulent atmosphere $T = 326.16$ $^\circ\text{K}$, we obtain $C_n = 0.75302 \times 10^{-6} C_T$ and $C_n^2 = 0.56704 \times 10^{-12} C_T^2$.

Discussion

In the above derivation, we assumed only the temperature dependence of refractive index of the atmosphere and neglected its pressure dependence. However, we may have to include some effect of pressure fluctuations. Since in case of sound waves, pressure effect is usually treated as an adiabatic process, it would be reasonable to assume that the pressure fluctuations induce the temperature fluctuations through the adiabatic thermodynamical process. Then, assuming the refractive index n is a function of the temperature T and pressure P and using a relation for the adiabatic process

$$\frac{dP}{dT} = \frac{\gamma}{\gamma-1} \frac{P}{T}, \quad (\gamma = C_p/C_v) \quad (17)$$

we obtain

$$C_n \text{ (adiabatic)} = \frac{77.6 P}{T^2} \frac{1}{\gamma-1} \left[1 + \frac{0.00753}{\lambda^2} \right] \times 10^{-6} C_T. \quad (18)$$

Inserting $\gamma = 1.40$ of the normal air, we obtain $C_n \text{ (adiabatic)} = 2.48 C_n$. Thus, it is essential for establishing the atmospheric model to compare the C_n directly measured by the optical method and the C_n obtained from C_T .

When the turbulence of the atmosphere is neither isothermal nor adiabatic process, we may have to include the pressure structure constant C_p and the pressure and temperature cross-structure C_{pT} . In case of the atmospheric turbulence in the

outside field, we must also include the effect of the humidity fluctuations and the density of other gases such as CO_2 .¹⁹

We would like to point out two interesting research areas pertinent to our turbulence experiment, although they are not directly related to the optical propagation. First, we may be able to clarify the physical meaning of non-gaussian statistics of temperature fluctuations exemplified in Figs. 10 and 11, by using some of the recent research results²⁰ on the temperature fluctuations. Second, by measuring the power spectrum of temperature fluctuations within the turbulent boundary layer, we may be able to determine the model of turbulence in the viscous-convective range. This is an interesting subject, because the "bump" in the power spectrum of temperature fluctuation, that is, the deviation from the $-5/3$ power law, have been observed in the atmospheric surface layer²¹ and is explained by the -1 power law for the viscous-convective range.^{22,23}

Two other methods for generating the isotropic and homogeneous turbulence have been reported: a "porcupine" like array of jet streams used by Betchov and Lorenzen²⁴ and the heated grid in a supersonic wind tunnel used by Shih-chun Lin and Shao-chi Lin.^{25,26} Compared to these methods, our turbulence chamber is much simpler to construct and more convenient to apply to the optical transmission measurements.

The performance of our turbulence chamber may be improved by some modifications: for instance, by adding the array of exhaust fans at the outlet, we should be able to widen the

region of uniform strength of turbulence. It is also desirable to channel the outlet flows to the air exhaust system in the laboratory, because even higher temperature setting of heater/blowers may be utilized. By making an array of holes on the walls, we may enhance temperature mixing and generate the stronger turbulence.

After the manuscript of this paper was prepared, we noticed an interesting, recent paper by Bissonnette²⁷ on the optical transmission in the aqueous turbulence with the specified strength of turbulence. The objective of the laboratory simulation described in the paper is very similar to ours. Our atmospheric turbulence chamber, however, has advantages such as convenience of inserting various optical and aerodynamical instruments in the chamber compared to the water chamber used by Bissonnette.

Conclusion

The average strength of refractive index fluctuations C_n^2 of the turbulent flow generated within the chamber was 10^3 times larger than that of the typical atmosphere in the field. The turbulence was locally homogeneous and isotropic within the region of 6 cm diameter. The average strength of turbulence was adequately homogeneous for the purpose of optical transmission measurements within the region 0.5 m x 0.05 m x 2 m at the standard optical height. Characteristic features of the generated turbulence are reproducible within the experimental errors. Various theoretical models of optical wave propagation in the turbulent atmosphere are being tested by using the laboratory generated turbulence with defined C_n^2 .²⁸ The determination of C_n^2 by irradiation fluctuation measurements will be described in a separate paper.

Acknowledgement

The authors wish to thank Profs. Paul D. Arthur and G. Scott Samuelsen (Mechanical Engineering Program, School of Engineering) for helpful discussions to define the critical Reynolds number of the turbulence chamber and to point out the mixing of two flows, one from the heater/blowers and the other, boundary shear flows at walls as origin of turbulence generation. This work was supported by the Air Force Office of Scientific Research (Grant 76-3097).

Appendix A: Measurement of Frequency Response of a Micro-Thermocouple by Using a Modulated Laser Beam.

A modulated 50 mW He-Ne 632.8 nm laser beam (single-mode, Spectra-Physics 125 A with Fabry-Perot Etalon in the cavity extender and Spectra-Physics 320 Modulator) was focused on micro-thermocouple junctions while the other junction was covered by a plastic case. The frequency response of the differential micro-thermocouple system was measured by taking the ratio of the output signal from the thermocouple system with those from a photomultiplier tube which detects the modulated laser beam directly. In order to determine the frequency response under the operating condition, the measurements were performed with heated air flow. The measured frequency response is shown in Fig. A1.

Appendix B: Evaluation of Average Temperature Gradient and
Characteristic Temperature From C_T^2

The temperature structure constant C_T^2 can be expressed as⁶

$$C_T^2 = \alpha^2 N / \varepsilon_T^{1/3} \quad (A1)$$

where the parameter α is given by the average energy dissipation rate ε and the kinematic viscosity ν as:

$$\alpha = \varepsilon_T / 3\nu \quad (A2)$$

A parameter N , which characterizes the intensity of the temperature fluctuations, is given by the thermal diffusivity χ and the mean square temperature gradient as

$$N = \chi \langle (\nabla T)^2 \rangle \quad (A3)$$

and

$$\chi = \kappa / \rho C_p \quad (A4)$$

where κ is the thermal conductivity, ρ is the density of the atmosphere and C_p is the constant pressure specific heat.²⁹

By inserting Eqs. (A2) and (A3) into Eq. (A1), we obtain

$$C_T^2 = \chi^6 (\Delta T)^2 / (9\nu^2 \varepsilon_T^{20/3}) \quad (A5)$$

The average thermal energy dissipation rate ϵ_T is given by

$$\epsilon_T = \chi^3 / \ell_0^4. \quad (\text{A6})$$

Since we determined $C_T^2 = 52.9^\circ\text{C}/\text{m}^4/3$ and $\ell_0 = 0.5$ cm, inserting $\chi = 0.200$ cm²/sec and $\nu = 0.1511$ cm²/sec, we obtain rms temperature gradient

$$\sqrt{\langle (\nabla T)^2 \rangle} = 1.898^\circ/\text{cm}. \quad (\text{A7})$$

The thermal diffusivity χ was obtained by inserting $\kappa = 2.6 \times 10^{-4}$ Watt/(cm²·c), $\rho = 1.2928$ g/liter and $C_p = 0.2398$ Cal/(g·°c) into Eq. (A4). By using Eq. (A6) and the thermal diffusivity χ_0 , we obtain average thermal energy dissipation rate ϵ_T :

$$\epsilon_T = 0.128 \text{ cm}^2/\text{sec}^3. \quad (\text{A8})$$

The characteristic temperature T_c of the turbulent temperature field is defined by the rms temperature gradient multiplied by the inner scale of turbulence ℓ_0 . (Ref. 6, p. 64). Using $\ell_0 = 5$ mm, we obtain characteristic temperature of our turbulence chamber $T_c = 0.949$ °K.

References:

1. B.L. McGlamery, J. Opt. Soc. Am. 57, 293-997 (1967).
2. Y. Kinoshita, H. Maeda and M. Suzuki, Proc. IEEE 56, 69-71 (1968).
3. M. Carnevale, B. Crosignani and P. Di Porto, Appl. Optics, 7, 1121-1123 (1968).
4. M. Bertolotti, M. Carnevale, B. Crosignani and P. Di Porto, Appl. Optics 8, 1111-1114 (1969).
5. O. Benda, G.D. Khoe and C. Nieuwvelt, Proc. IEEE 61 684-685 (1973).
6. V.I. Tatarski, "The Effects of the Turbulent Atmosphere on Wave Propagation," (TT-68-50464), National Science Foundation, Washington, D.C., distributed by National Technical Information Service, 5282 Port Royal Rd., Springfield, VA 22151 Section 13, The Microstructure of the Temperature Field in Turbulent Flow (1971).
7. A.M. Yaglom, Doklady Akad. Nauk. USSR 69, 743 (1949).
8. J.E. Pearson, J. Opt. Soc. Am. 65, 938 (1975).
9. S. Corrsin, J. Aero Sci. 17, 417 (1950).
10. S. Corrsin, J. Appl. Phys. 22, 496 (1951).
11. H. Schlichting, "Boundary Layer Theory," translated by J. Kestin, McGraw-Hill Book Co. (1968). Also German edition by the same author, "Grenzschicht-Theorie," Verlag G. Braun, Karlsruhe (1950).
12. J.K. Vennard and R.L. Street, "Elementary Fluid Mechanics," John Wiley and Sons, Inc. (1975).

13. G.K. Batchelor, "Theory of Homogeneous Turbulence," Univ. Press, Cambridge (1960).
14. John W. Strohbehn, Progress in Optics 9, 73-122 (1971).
15. Harold Cramer, "Mathematical Methods of Statistics," Princeton University Press, Princeton, N.J. (1951).
16. M.G. Kendall and A. Stuart, "The Advanced Theory of Statistics, Vol. 1, Distribution Theory," Hafner Publ. Co., New York (1969)
17. D. Atlas, R.M. Cunningham, R.J. Donaldson, Jr., G. Kantor and P. Newman, "Some Aspects of Electro-Magnetic Wave Propagation, " Chap. 9, Handbook of Geophysics and Space Enviornments, edited by S.L. Valley, Air Force Cambridge Research Laboratories (1965).
18. G.R. Ochs, R.R. Bergman and J.R. Snyder, J. Opt. Soc. Am. 231-234 (1969).
19. C.A. Friehle, J.C. LaRue, F.H. Champagne, C.H. Gibson and G.F. Dryer, J. Opt. Soc. Am. 65, 1502-1511 (1975).
20. R.A. Antonia, Physics of Fluids 18, 1584-1585 (1975).
21. Champagne, F.H., C.A. Friehe, J.C. LaRue and J.C. Wyngaard, J. Atmos. Sci. 34, 515-530 (1977).
22. R.J. Hill and S.F. Clifford, Topical Meeting on Optical Propagation Through Turbulence, Rain and Fog, Optical Society of America, Aug. 9-11, 1977, Boulder, CO.
23. R.J. Hill, Physics of Fluids, to be published.
24. R. Betchov and C. Lorenzen, Physics of Fluids, 17, 1503-1508 (1974).

25. Shih-chun Lin and Shao-chi Lin, *Physics of Fluids*, 16, 1587-1598 (1973).
26. Shao-chi Lin and Shih-chun Lin, *Physics of Fluids*, 19, 1099-1108 (1973).
27. L.R. Bissonnette, *Appl. Optics* 16, 2242-2251 (1977)
28. Arun K. Majumdar, Ph.D disseration, University of California, Irvine, June 1977 (Appendix C)
29. American Institute of Physics Handbook, 3rd Ed. P. 4-144, McGraw Hill Book Co., (1972).

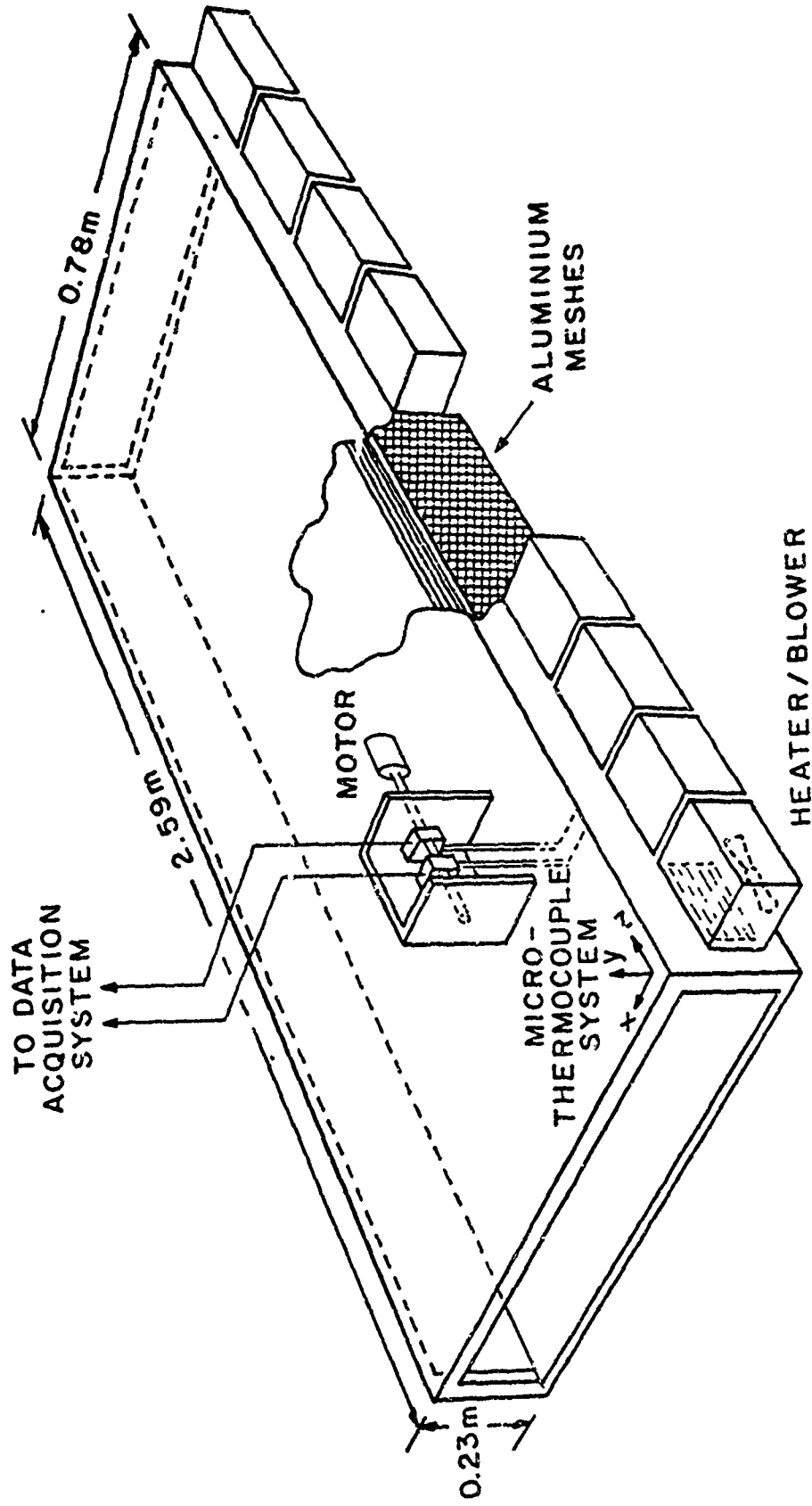


Fig. 1. Schematic diagram of the turbulence chamber including the micro-thermocouple system.

(31)

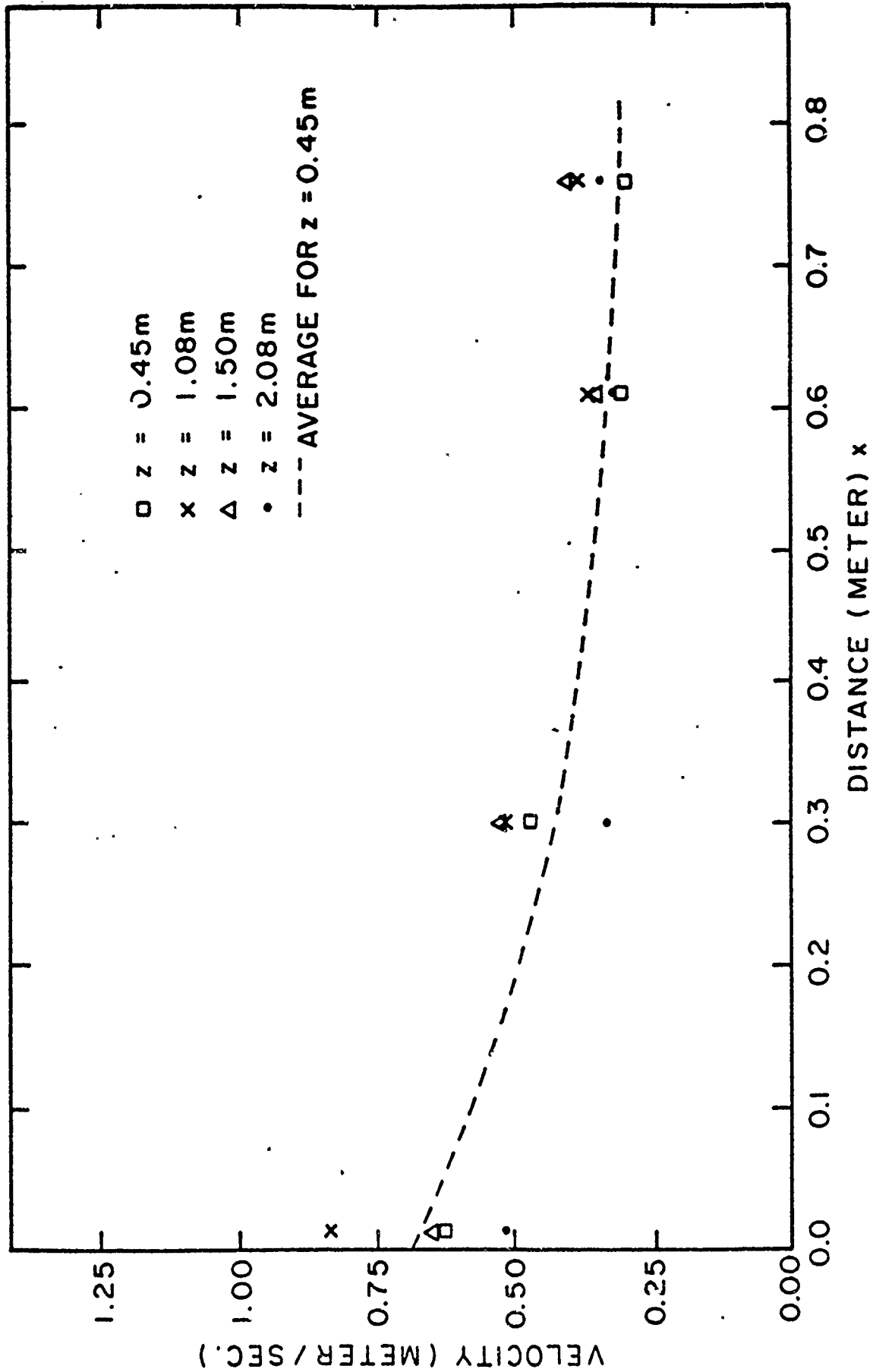


Fig. 2. Average wind velocity within the turbulence chamber is shown as a function of the distance x from the last screen along the direction of air flow.

(32)

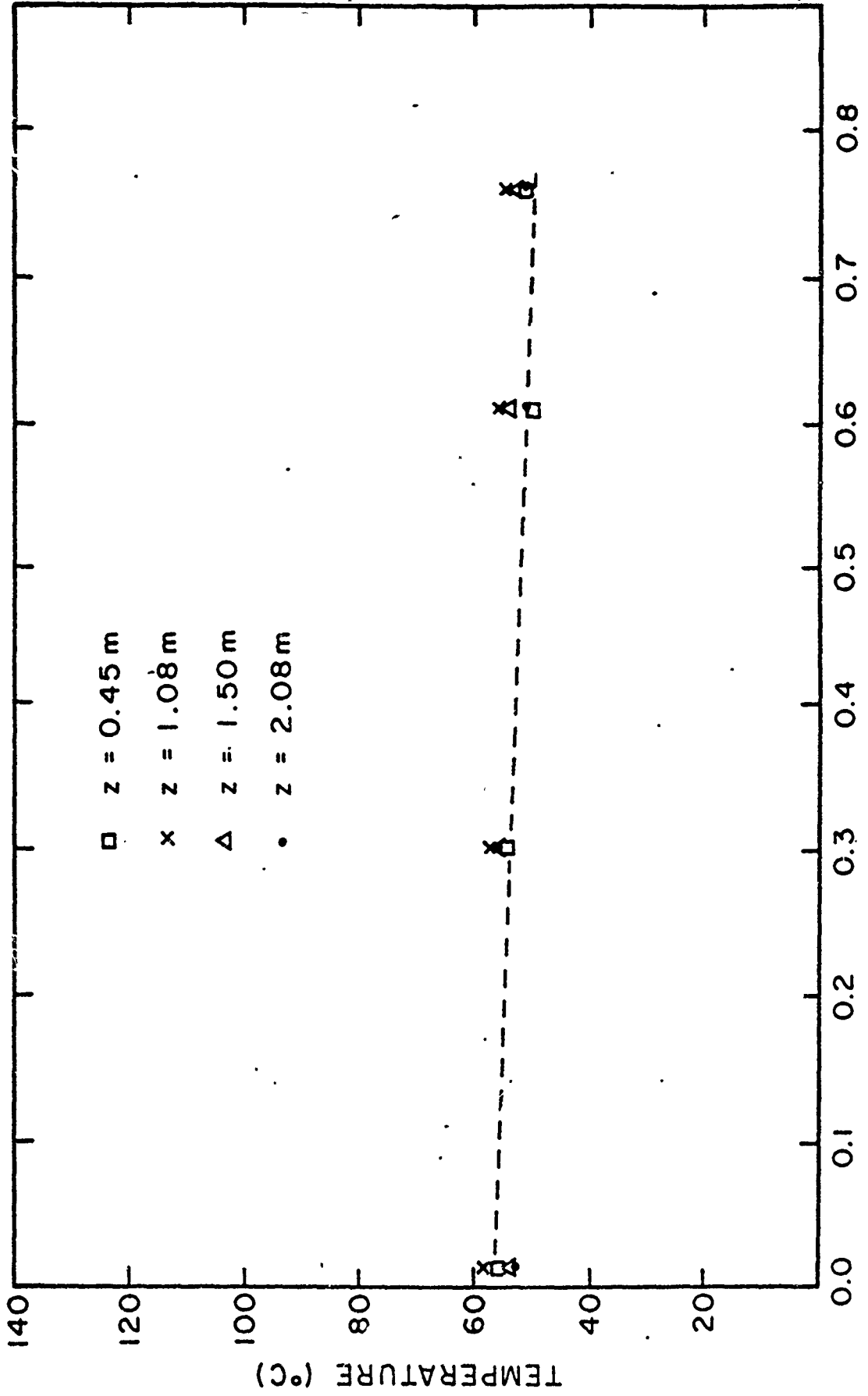


Fig. 3. Average air temperature within the turbulence chamber is shown as a function of the distance x from the last screen along the direction of air flow.

(33)

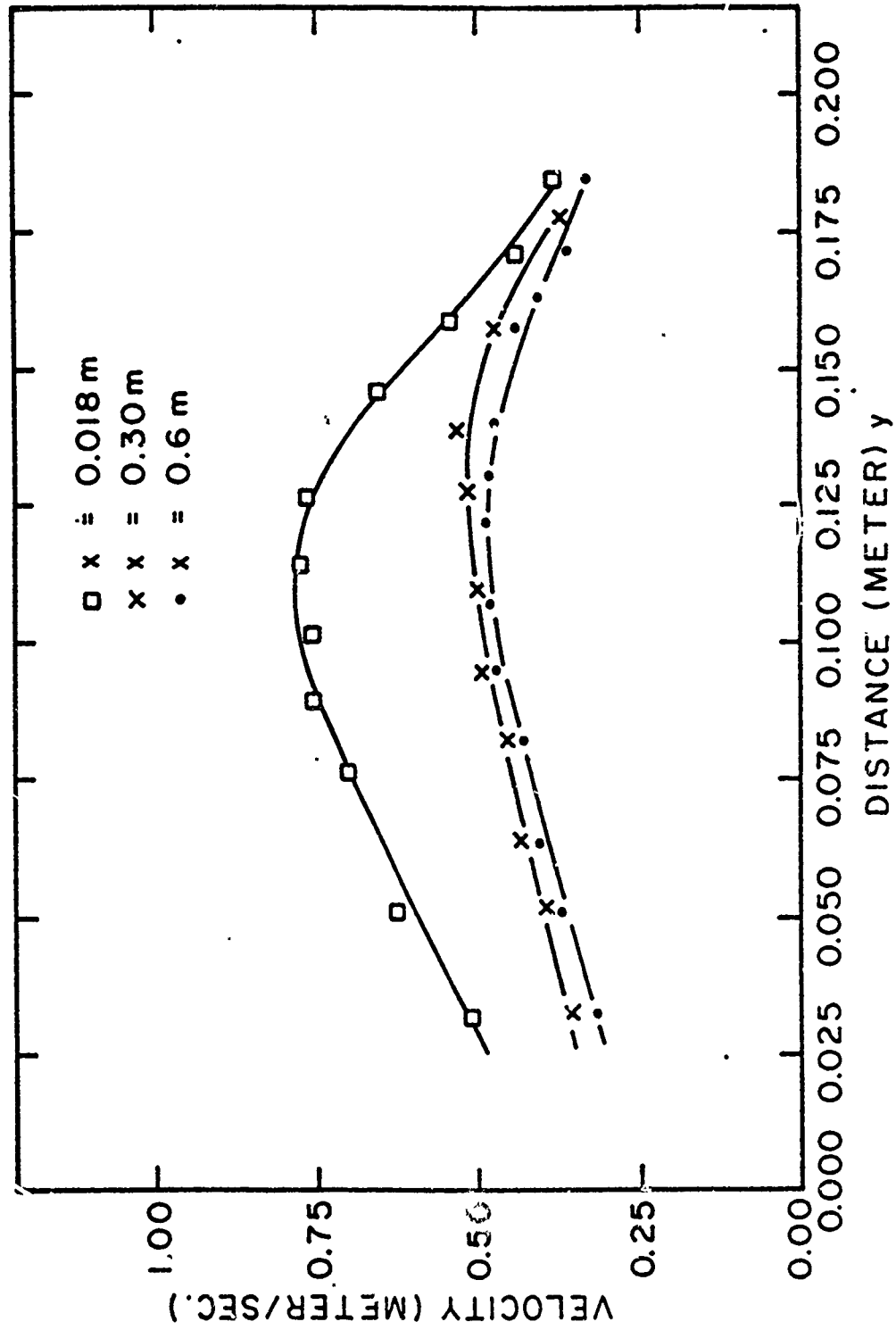


Fig. 4. Average wind velocity within the turbulence chamber is shown as a function of the height y with respect to distance $x = 60$ cm.

(34)

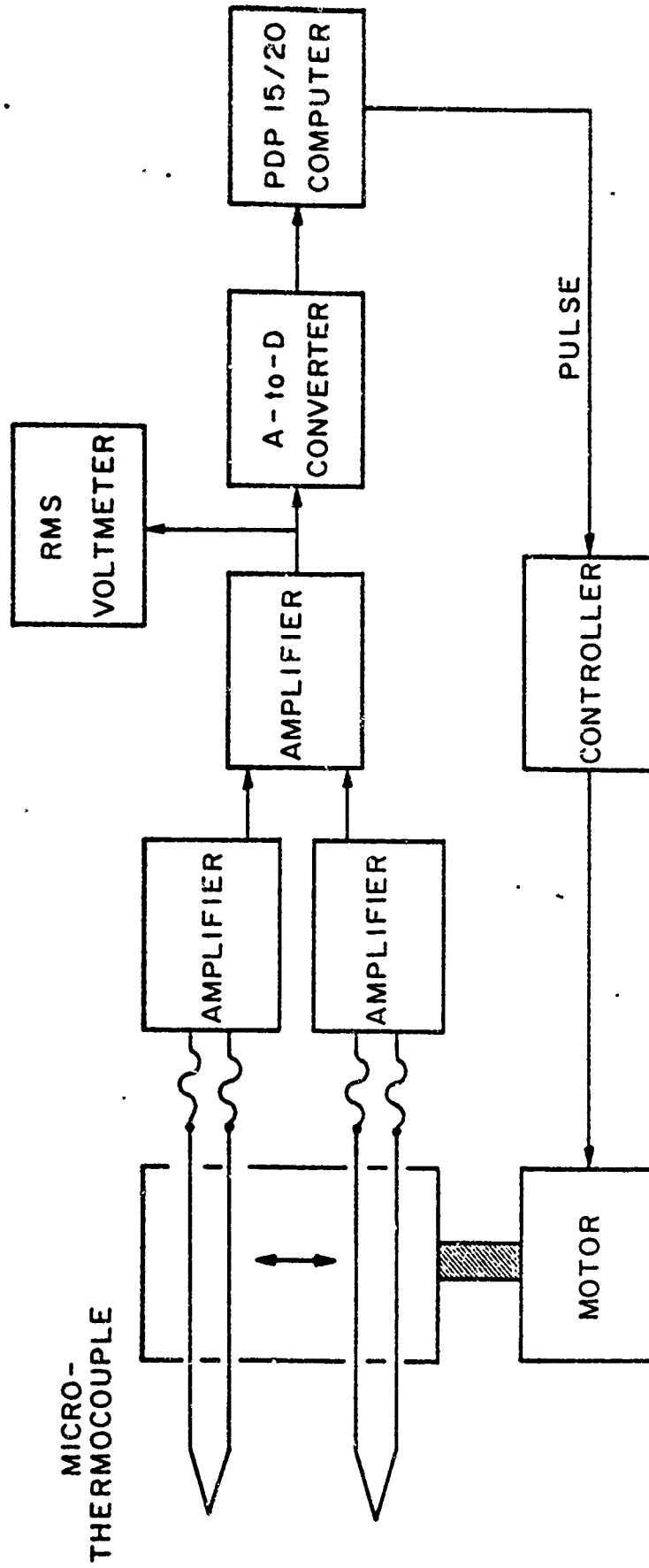


Fig. 5. Schematic diagram of measurement system of temperature structure function by micro-thermocouples.

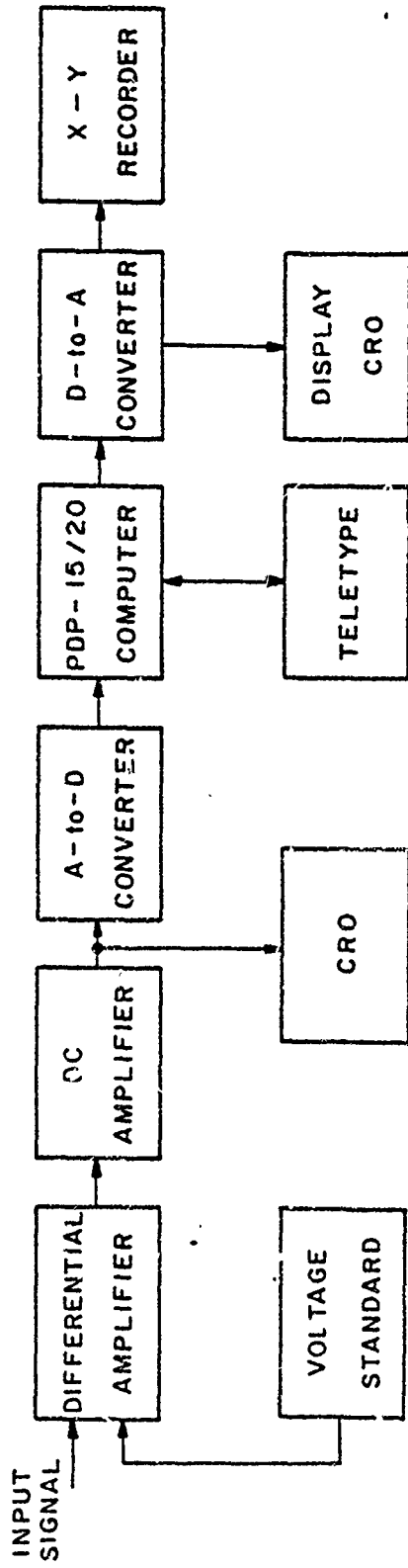


Fig. 6. Statistical data acquisition system used for measuring the temperature structure function, histogram and cumulants and power spectrum of temperature fluctuations.

(36)

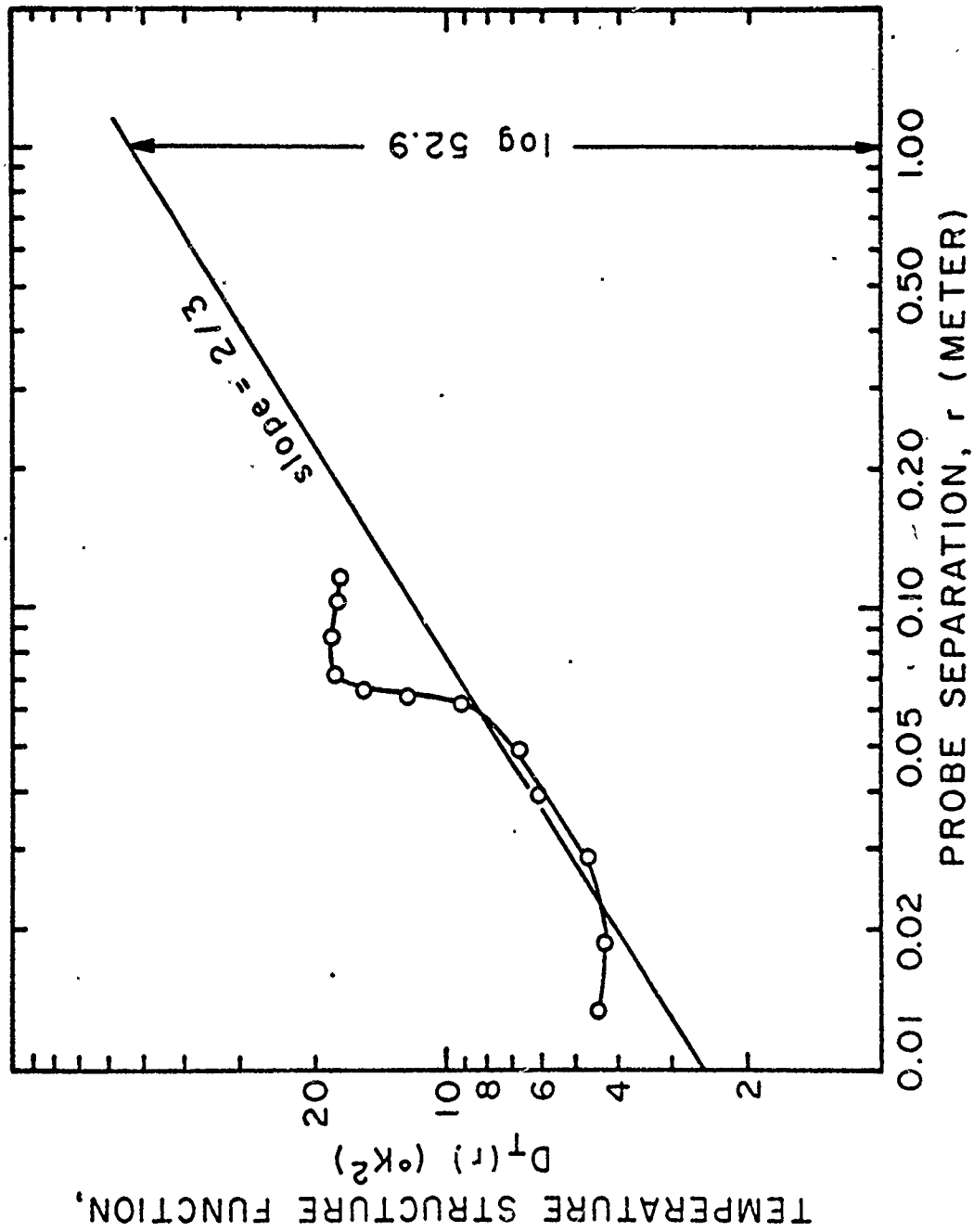


Fig. 7. Temperature structure function $D_T(r)$ vs micro-thermocouple probe separation r , where the slope $2/3$ line and C_T^2 determined as the value at $r = 1$ are indicated.

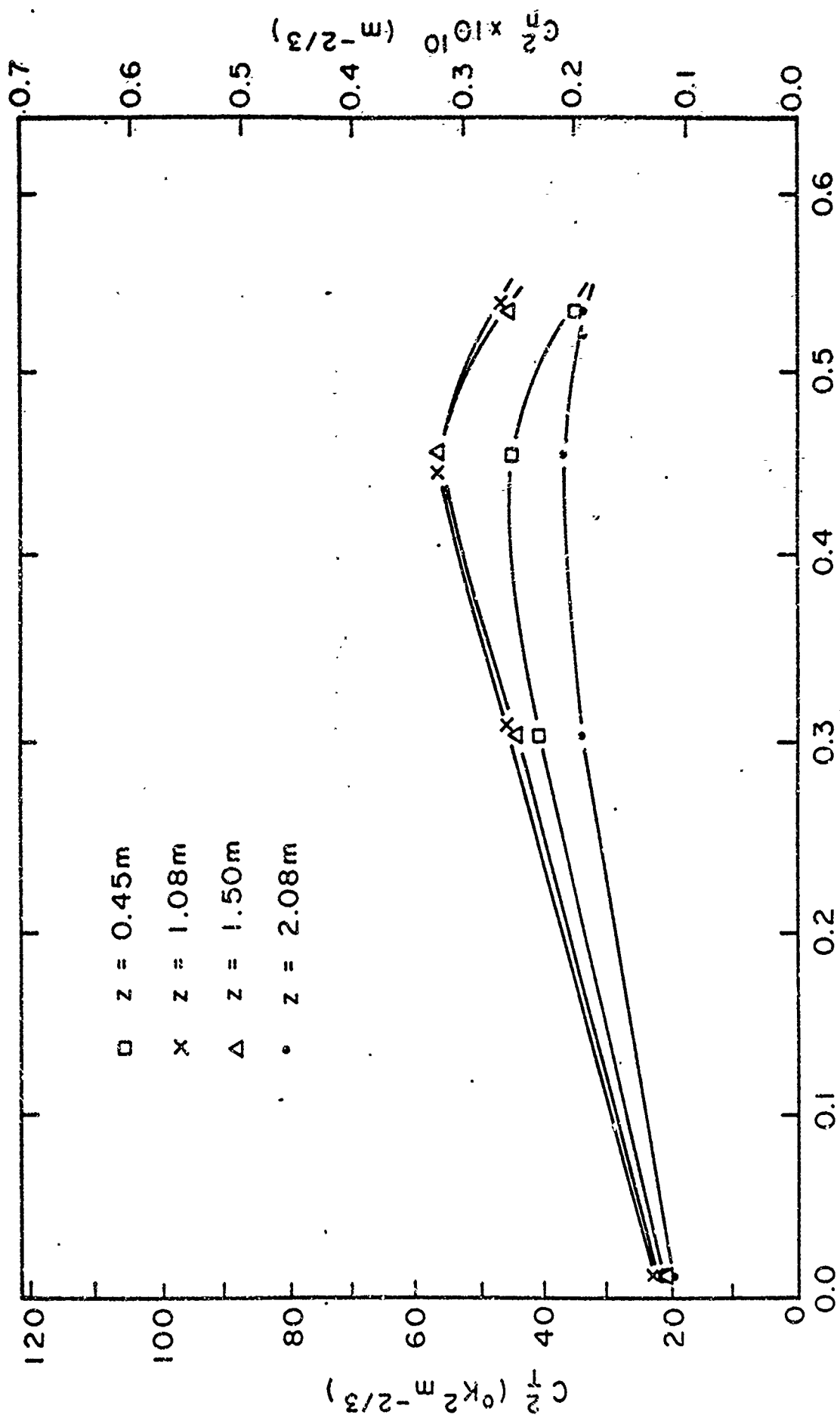


Fig. 8. Refractive index structure constant squared C_n^2 and temperature structure constant squared C_t^2 vs distance x from the last screen along the direction of air flow

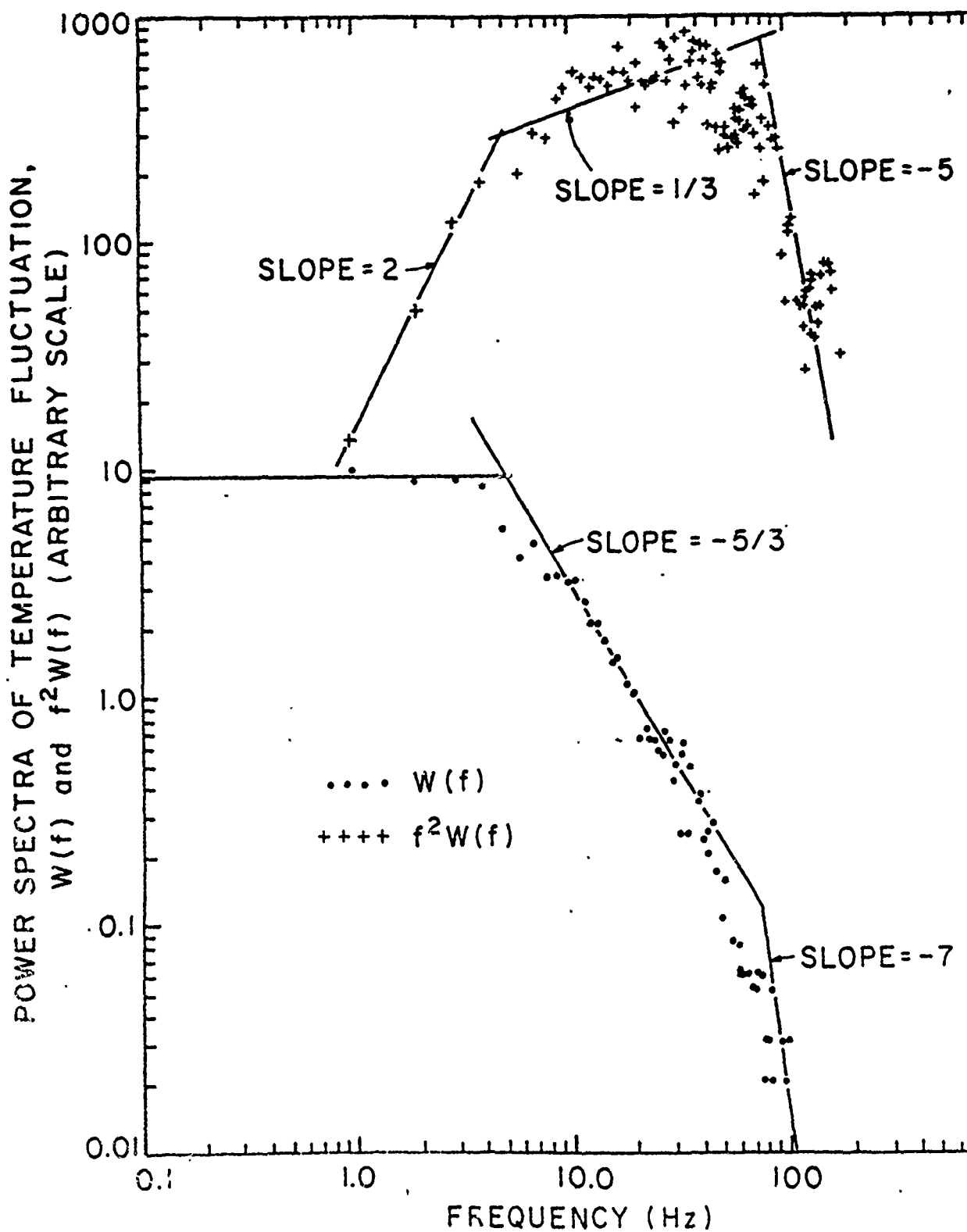
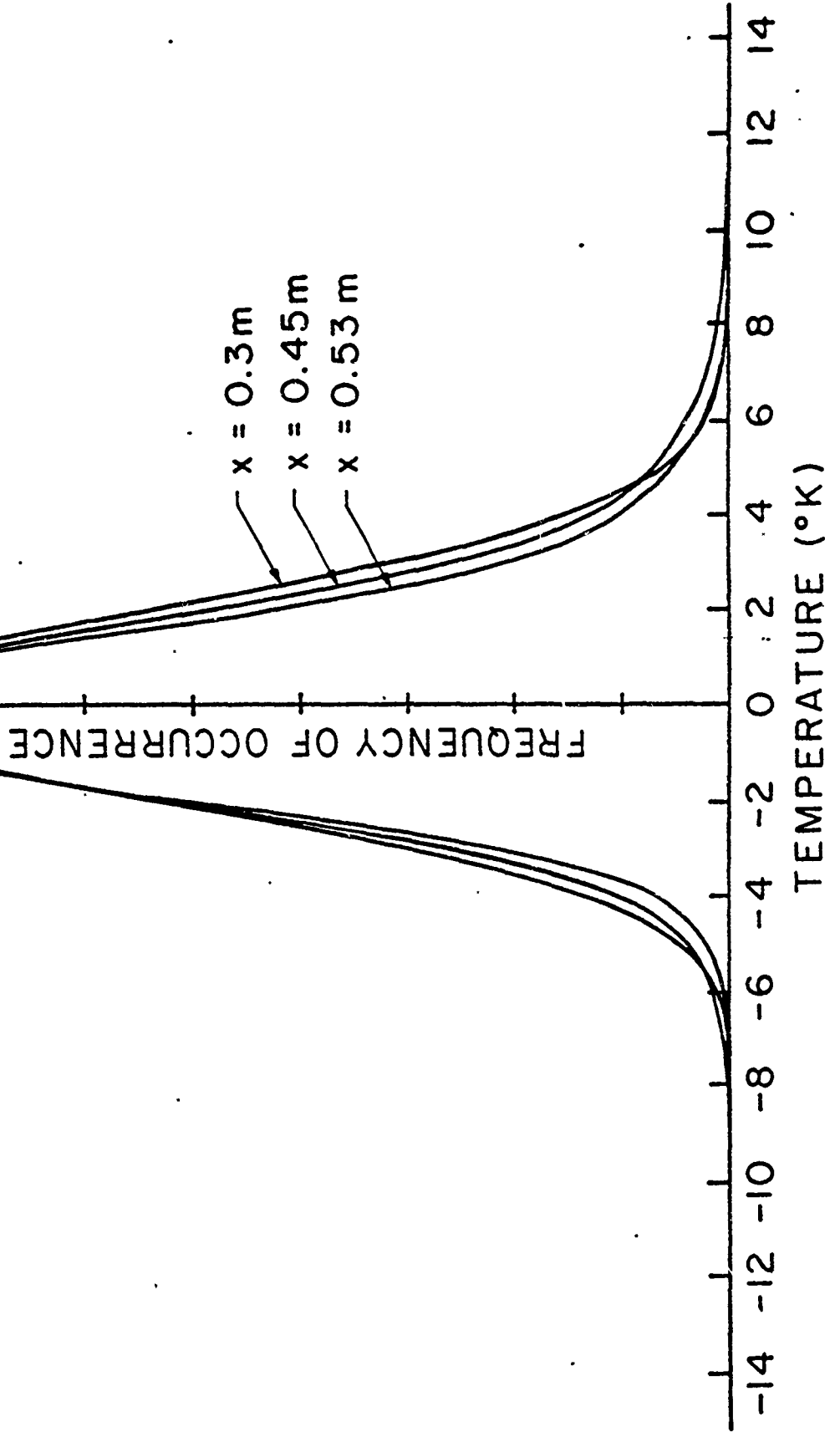


Fig. 9. Power spectrum of temperature fluctuation $W(f)$ and $f^2W(f)$ are shown as a function of frequency (Hz) where slopes of respective regions are indicated.

(39)

Fig. 10. Normalized histograms of temperature fluctuations measured for distance x from the last screen along the direction of air flow.



(40)

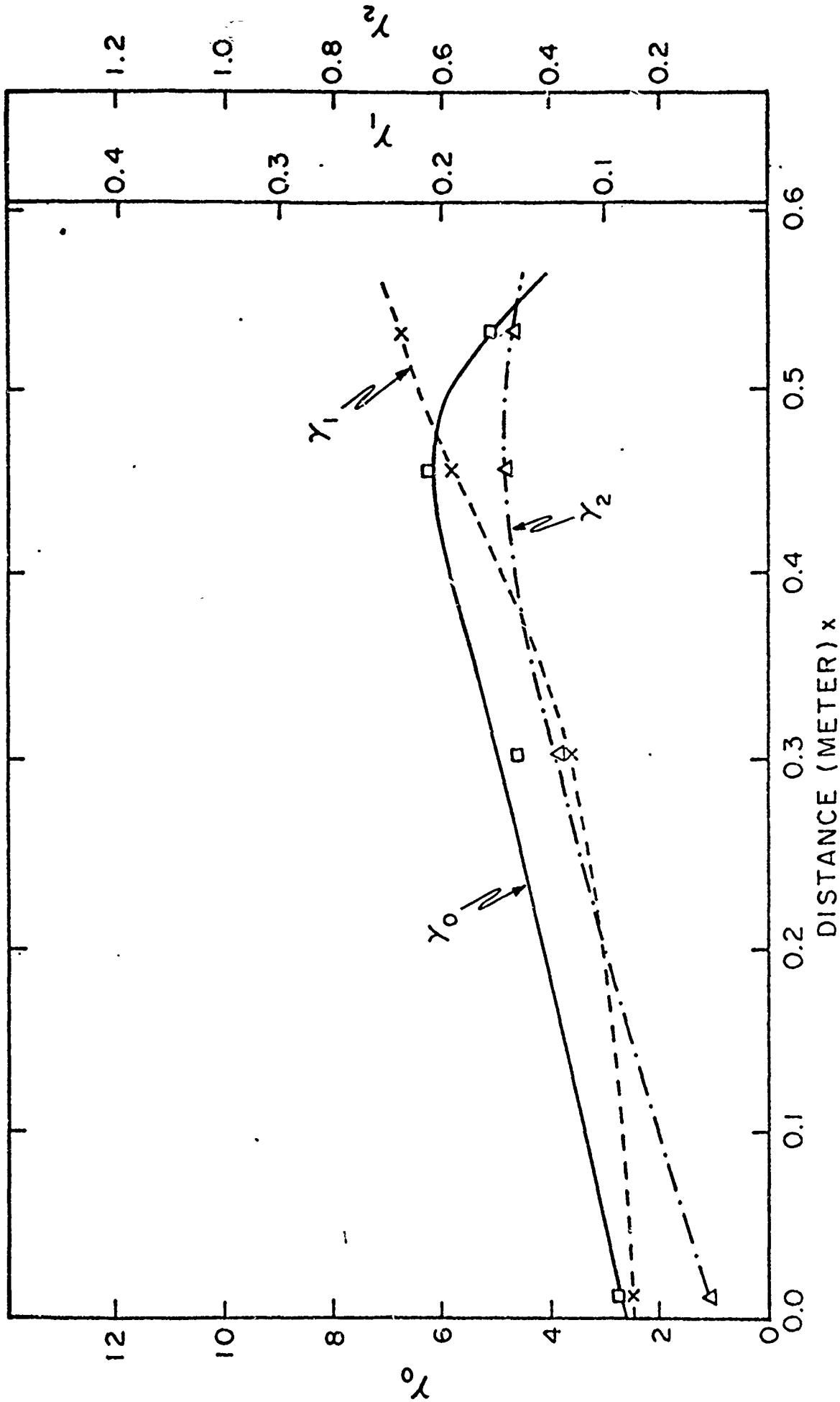


Fig. 11. Coefficients of variation, skewness and excess of temperature fluctuations are shown as functions of the distance x from the last screen along the direction of turbulent air flow.

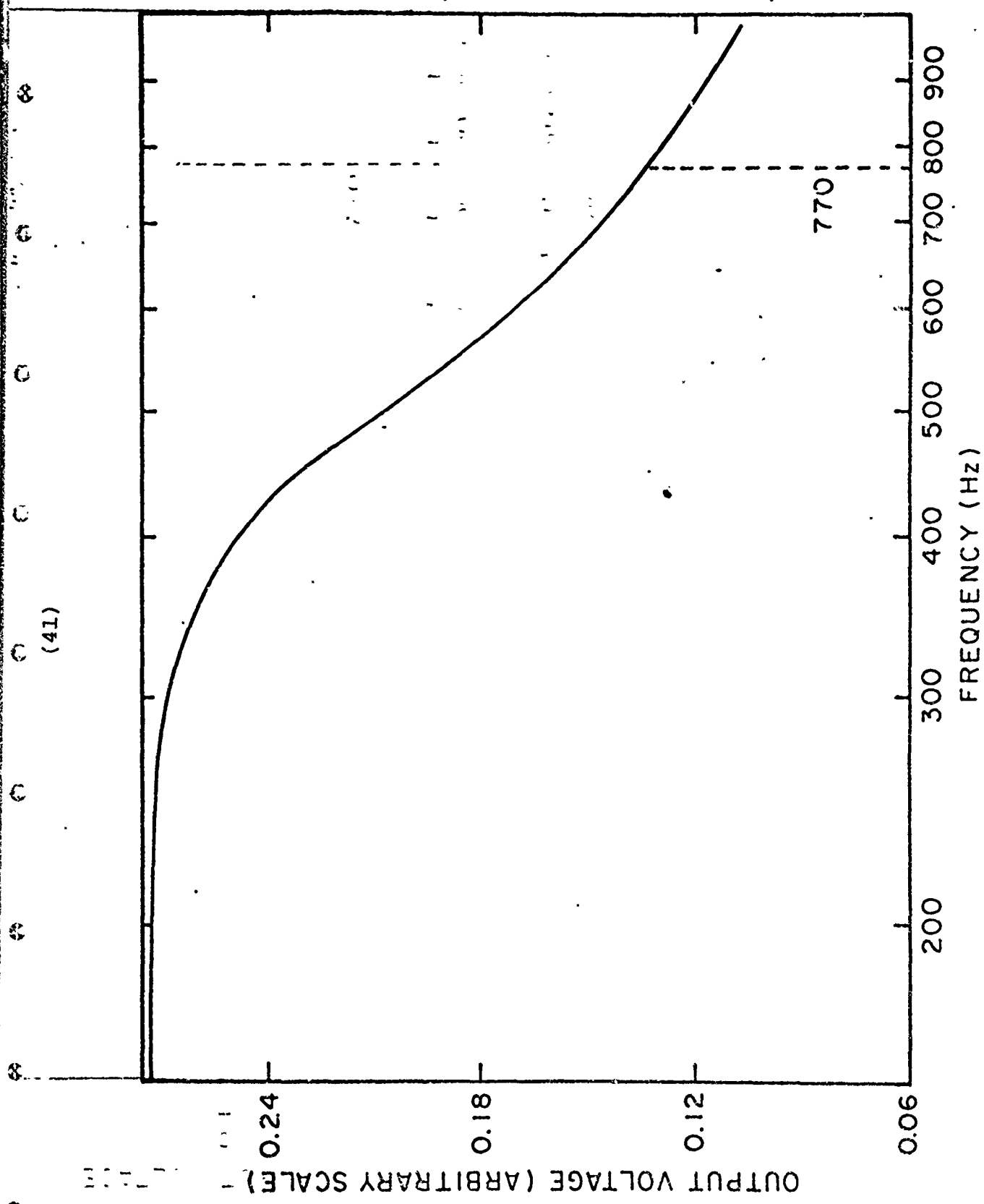
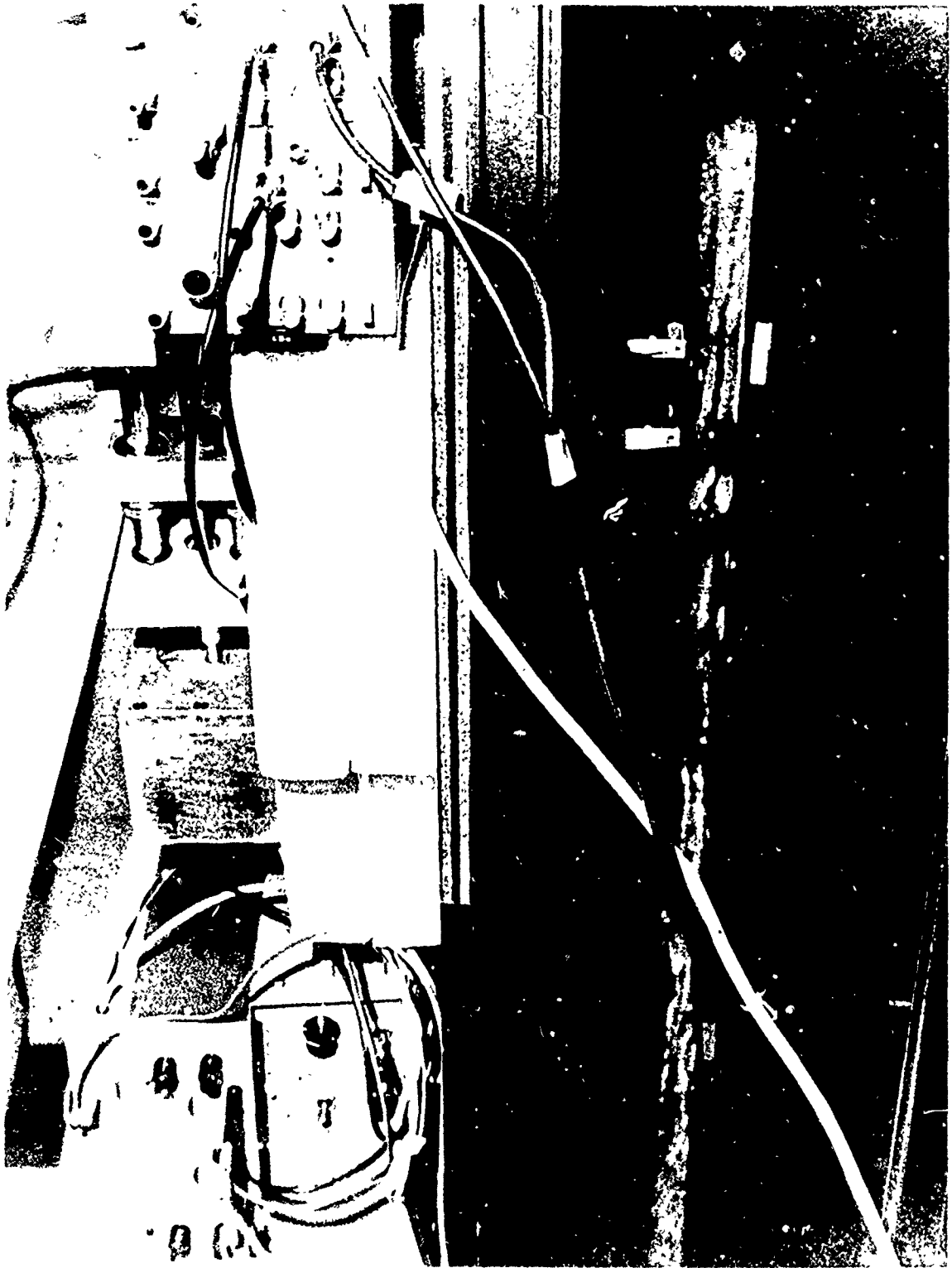


Fig. A1. The output voltage of the thermocouple systems, normalized by the intensity of modulated laser beams is shown as a function of frequency (Hz).



MEASUREMENT OF C_T^2 USING A PAIR OF MICROTHERMO-COUPLES

APPENDIX II

COMPARISON OF A CORNER-CUBE REFLECTOR AND A PLANE MIRROR
IN FOLDED PATH AND DIRECT TRANSMISSION
THROUGH ATMOSPHERIC TURBULENCE

INTRODUCTION

The objective of the experiment was to clarify the different characteristics of folded transmission by a corner-cube reflector and a plane mirror through the atmospheric turbulence,¹ and also to establish theoretical models for characterizing the irradiance fluctuations measured for these cases. Due to the unpredictable conditions of the real atmosphere, we have emphasized on the experiments performed by using an atmospheric turbulence chamber, which can generate a locally isotropic and homogeneous turbulence in the laboratory. The results of the field experiments is also described.

EXPERIMENTAL SET-UP FOR THE LABORATORY EXPERIMENTS

The experimental set-up is shown in Fig. 1. A collimated laser beam with the diameter of cross-section 2.54 cm from a single-mode He-Ne gas laser (Spectra Physics 119, 6328 A) was used for the laboratory experiments using an atmospheric turbulence chamber. A corner-cube reflector with the diameter 2.22 cm and a front surface aluminized plane mirror of the size 4.45 cm x 2.54 cm with $\lambda/4$ flatness were used for these experiments.

The light beams transmitted through the turbulent atmosphere were detected by a photomultiplier tube (IP21) with an entrance diaphragm of one mm diameter, and the output voltage from the detector was amplified by two cascaded DC amplifiers and then was converted into the digital form by an Analog-to-Digital convertor (Preston Scientific, 14 bits, plus sign and 100 KC sampling rate.) The digital signals thus obtained were processed by a digital data acquisition system (PDP 15/20 with 24 K core memory.) The temporal frequency spectra of irradiance fluctuations were obtained by using the Fast Fourier Transform method and histograms of irradiance fluctuations were obtained and various moments, central moments and cumulants were determined from these histograms (See Fig. 2.) The turbulence chamber² with internal dimensions, 2.59 m long, 0.78 m wide and 0.23 m high was assembled on a shock-mounted optical bench (See Fig. 3.) The heated turbulent flow was generated by ten small electric heaters with blowers. The average transverse wind velocity at the standard optical height 0.12 m was 0.41 m/sec, and the average temperature was 53° C.

The Reynolds number of this chamber was estimated as 6287 with the separation between upper and lower plates 0.23 m and the kinematic viscosity of the air $\nu = 1.5 \times 10^{-5} \text{ m}^2/\text{sec}$. The value exceeds the critical Reynolds numbers for the flow between parallel walls. The turbulence generated was locally homogeneous and isotropic within a sphere of 6 cm diameter. The

average strength of turbulence was adequately homogeneous for this optical measurement within the region $0.5 \times 0.005 \times 2$ m at the standard optical height. The average strength of refractive index fluctuations C_n^2 was $2.65 \times 10^{-11} \text{ m}^{-2/3}$. The inner scale l_0 and outer scale of turbulence L_0 were estimated as $l_0 = 5$ mm and $L_0 = 8$ cm, respectively.

RESULTS OF LABORATORY EXPERIMENTS

The normalized power spectrum of irradiance fluctuations measured was flatter and broadened for the corner-cube reflector and was sharper for the plane mirror reflector. The power spectrum of irradiance fluctuations in the plane mirror reflector was broader than that of the corner-cube reflector case. The histograms of corner-cube reflector are closer to the direct transmission of the same transmission path length. The statistical quantities measured, the coefficients of variation (γ_0), skewness (γ_2) as well as the quantity $f_0 \sqrt{2\pi \lambda L} / V$ and frequency bandwidth Δf are summarized in Table 1, where the critical frequency $f_0 = V / \sqrt{2\pi \lambda L}$, V the average transverse wind velocity, λ the wavelength of light and L the path length. The histograms obtained are shown in Fig. 4

FIELD EXPERIMENTS

A similar experiment was carried out in a real turbulent atmosphere (one way path length 274 m) on the night of Dec. 14, 1976. The wind velocity was approximately 3 miles per hour.

The results are summarized in Table 2.

The profile of the height of transmitted beam is illustrated in Fig. 5.

DISCUSSIONS

The experimental results of histograms may be qualitatively explained by considering the fact that the forward and backward transmission through turbulent atmosphere are somewhat correlated in the case of corner-cube reflector, whereas the transmission of incident and reflected beams through turbulent atmosphere will be statistically more independent.

With regards to the peak frequency f_0 of the normalized power spectrum of irradiance fluctuations, the experimental results may be explained by considering the fact that since the beams diffracted by small eddies tend to go outside of the light receiver in the folded path, the lower frequency components due to the larger eddies will be emphasized in the folded path experiment than in the direct path experiment.³ In case of corner-cube reflector, the high frequency components due to the small eddies will be scattered more than single plane mirror reflection and its high frequency irradiance fluctuations will be smoothed out.

The frequency bandwidths of irradiance fluctuations in folded path cases may be explained by considering the Doppler shift, because the positively Doppler shifted components will

be further shifted to the higher frequency and the negatively shifted components will be further negatively shifted in case of a plane mirror reflection. Whereas, in the corner-cube reflector, the frequency shift of the reflected beam will be in the opposite direction. (See Fig. 6 and 7). In other words, the positively shifted components in one way will be negatively shifted in return. Hence, the over-all frequency shift will be smaller in corner-cube reflector than the case of a plane mirror reflector.

By using the angle of incidence fluctuations, we should be able to formulate the power spectra of irradiance fluctuations in corner-cube and plane mirror reflectors.

REFERENCES

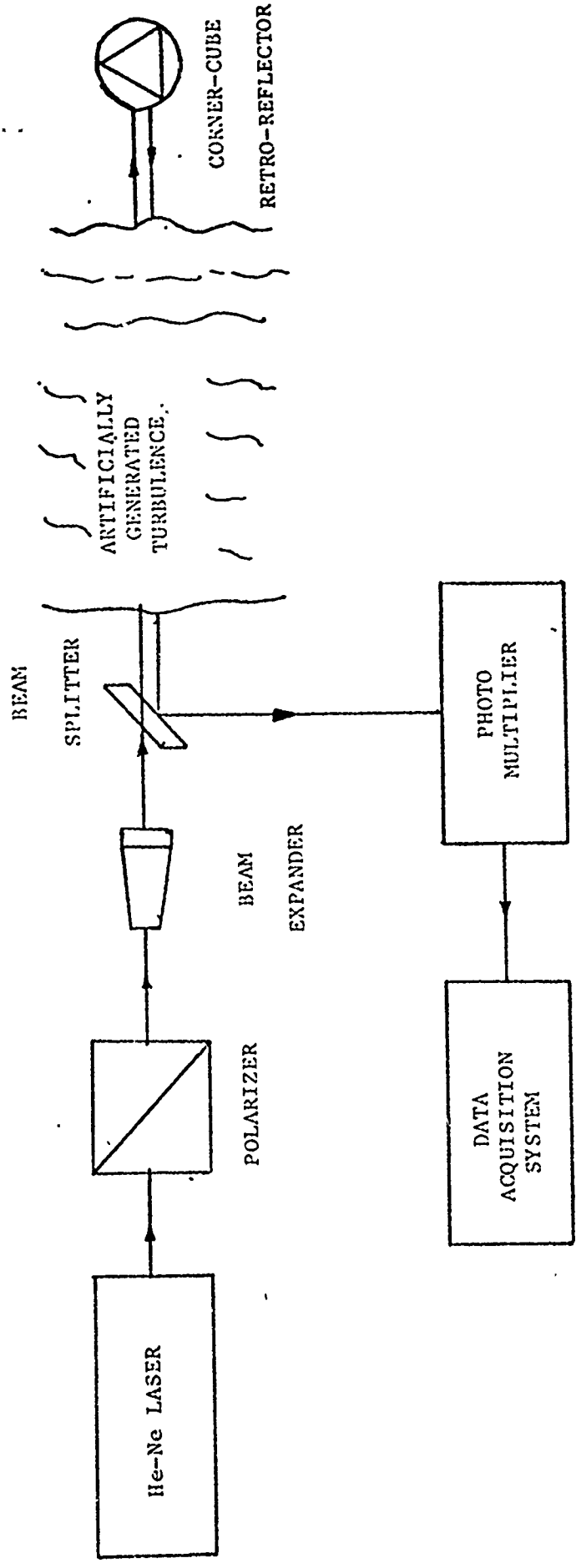
1. Majumdar, A. K. and Gamo, H., J. Opt. Soc. Am. 66, 1067 (1976).
2. Majumdar, A. K., "Statistical Characteristics of Laser Propagation Through Laboratory Generated Atmospheric Turbulence," Ph. D. Dissertation, June 1977.
3. Smith, J. and Pries, T. H., Appl. Opt. 14, 1161 (1975).

	<u>Statistical quantities</u>			peak frequency f_o/f_c	band- width Δf HZ
	γ_0	γ_1	γ_2		
Direct Collimated Laser, path length = 2.54 m	0.054	0.310	0.886	0.201	28
Corner-Cube at 1.27 m	0.012	0.278	0.915	0.184	26
Plane Mirror at 1.27 m	0.007	0.187	1.378	0.197	38
Corner-Cube at 2.54 m	0.025	0.560	0.401	0.126	38
Plane Mirror at 2.54 m	0.103	0.792	1.394	0.140	50

TABLE I. Comparison of measured quantities for corner-cube plane mirror and direct path where f_o measure peak frequency of normalized power spectrum and Tatarski's critical frequency $f_c = v_{\perp} / \sqrt{2\pi \lambda L}$.

	<u>Statistical quantities</u>			f_o/f_c
	γ_0	γ_1	γ_2	
Direct collimated laser, path length = 274 m	0.383	0.124	0.205	0.886
Folded path via corner- cube, one way path = 274 m	0.383	0.592	0.744	0.699
Folded path via plane mirror, one-way path = 274 m	0.989	0.695	0.787	0.801

Table II. Comparison of measured quantities for corner-cube plane mirror and direct path, where f_c is the Tatarski's critical frequency $v \perp / \sqrt{2\pi \lambda L}$.



SCHEMATIC DIAGRAM OF EXPERIMENT

FIGURE 1

(51)

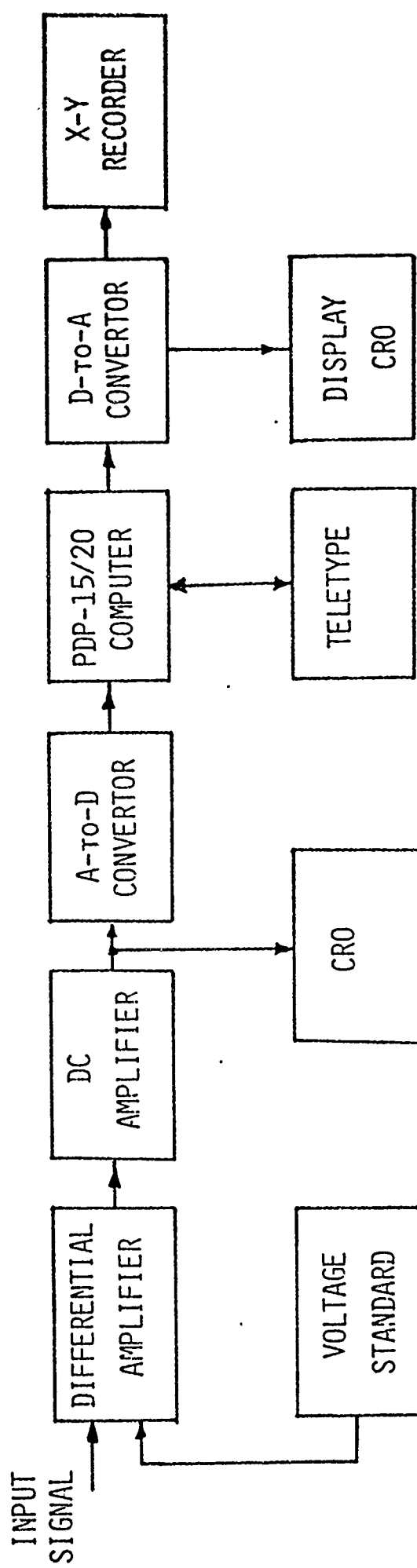
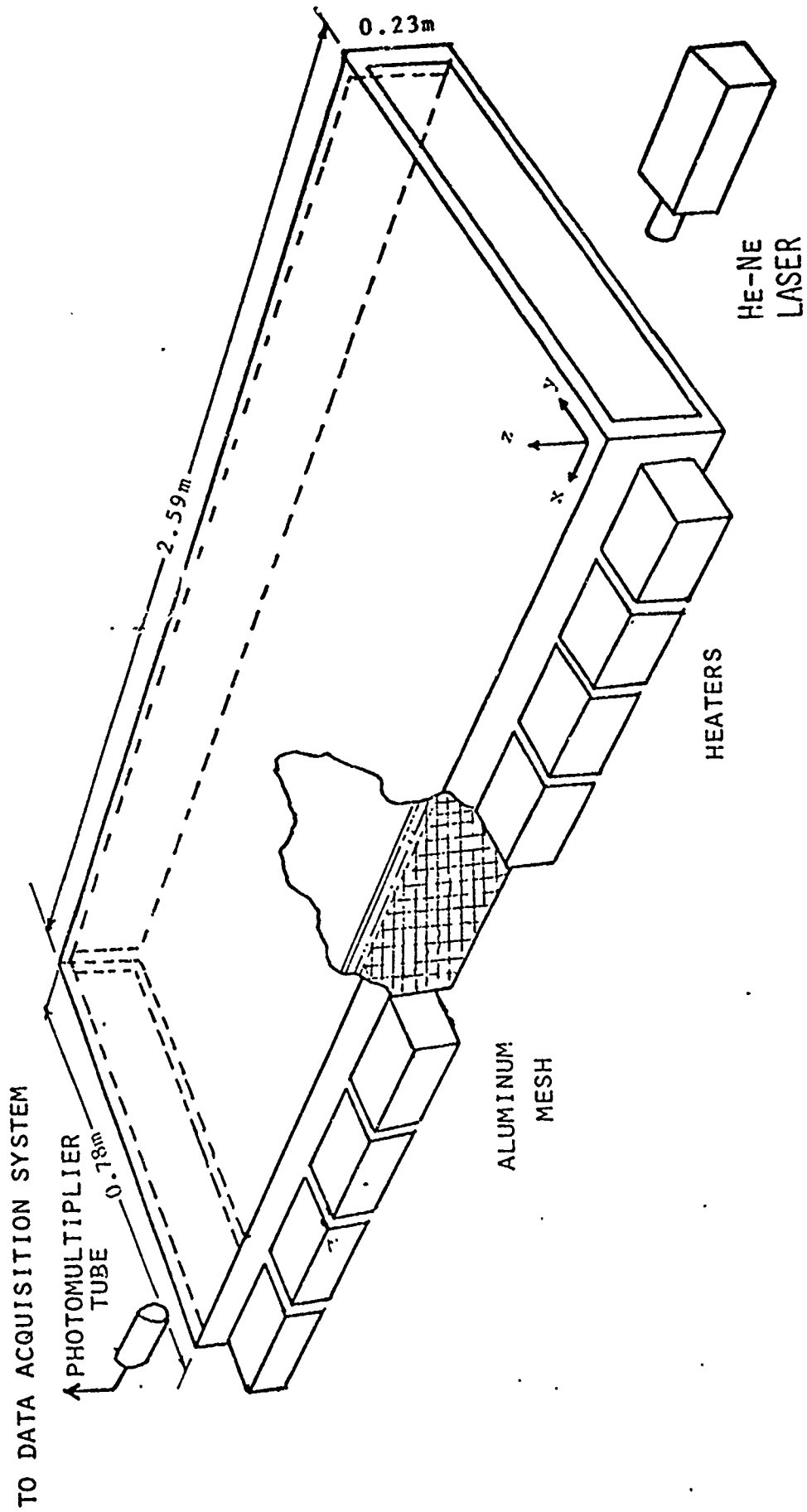


FIGURE 2

DATA ACQUISITION SYSTEM FOR OPTICAL METHOD



: EXPERIMENTAL ARRANGEMENTS FOR MEASURING IRRADIANCE FLUCTUATIONS BY OPTICAL METHOD

FIGURE 3

FREQUENCY HISTOGRAM

(53)

PLANE MIRROR 2 WAY
CORNER-CUBE 2 WAY
DIRECT 1 WAY

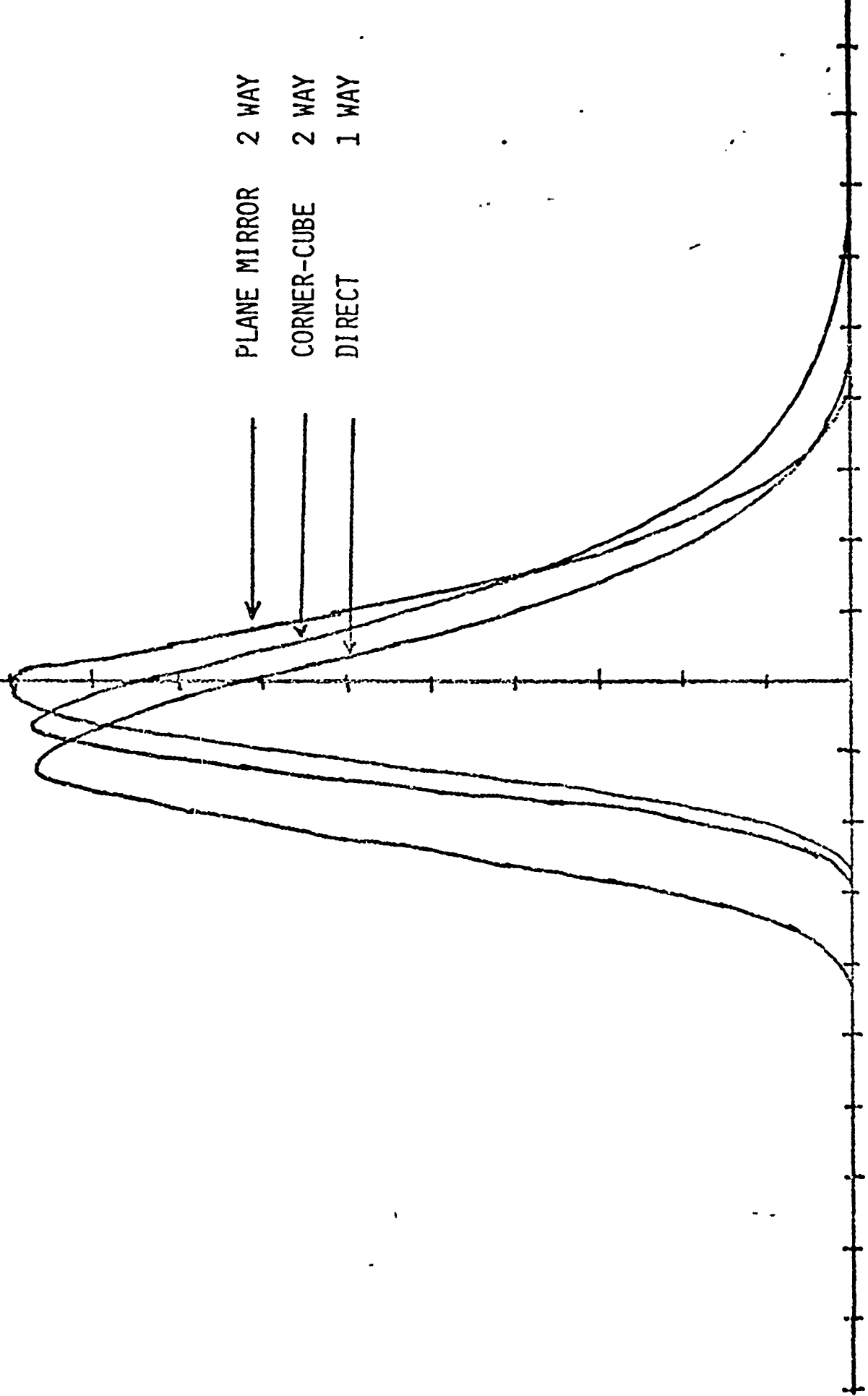


FIGURE 4

(54)

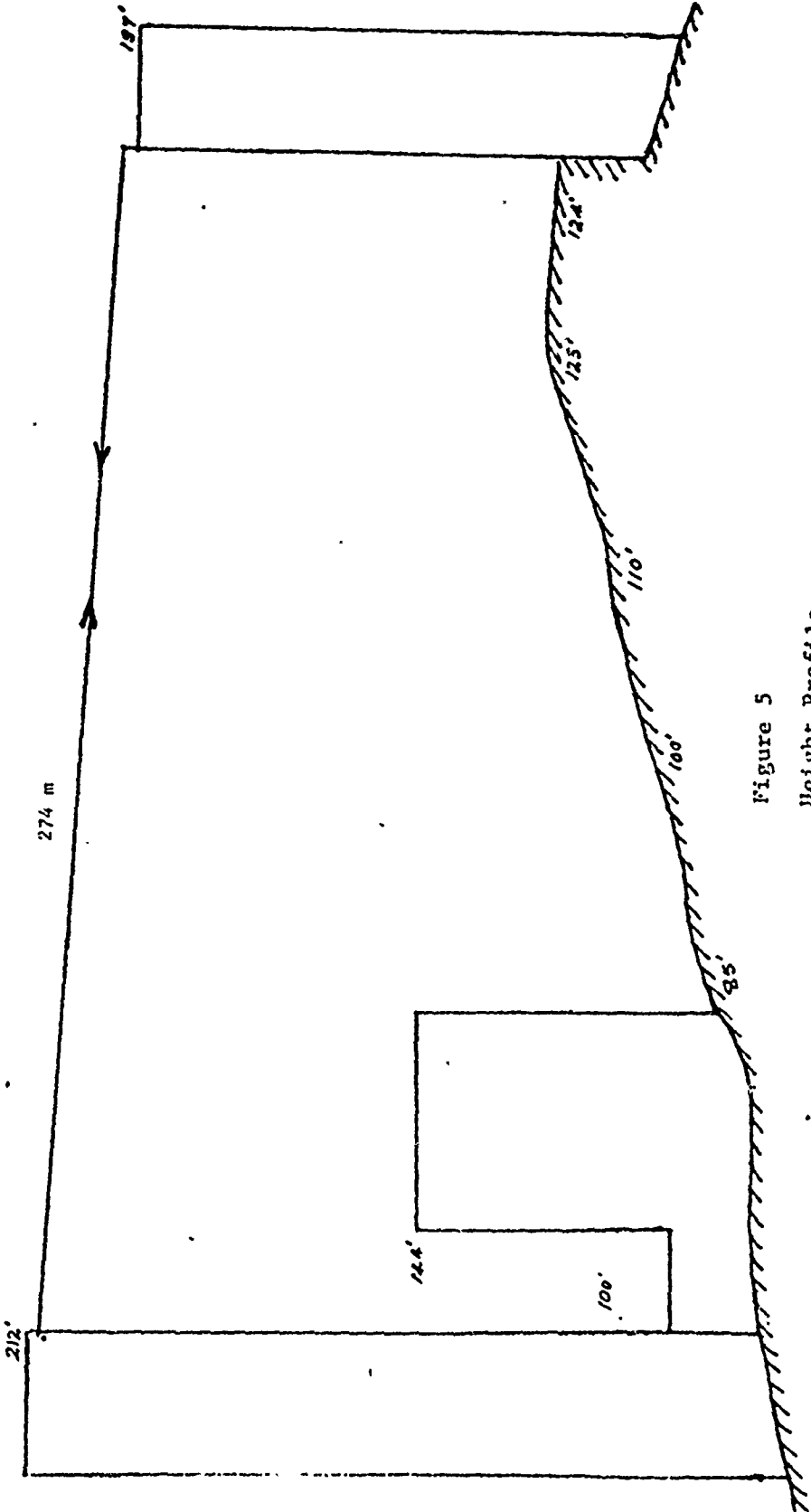


Figure 5
Height Profile

PLANE-MIRROR REFLECTION

(55)

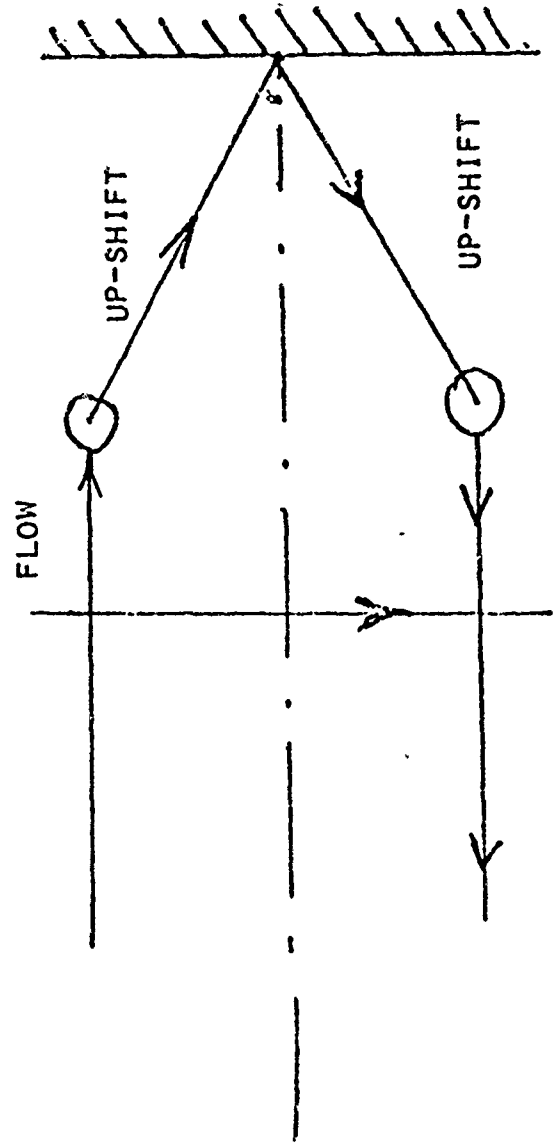
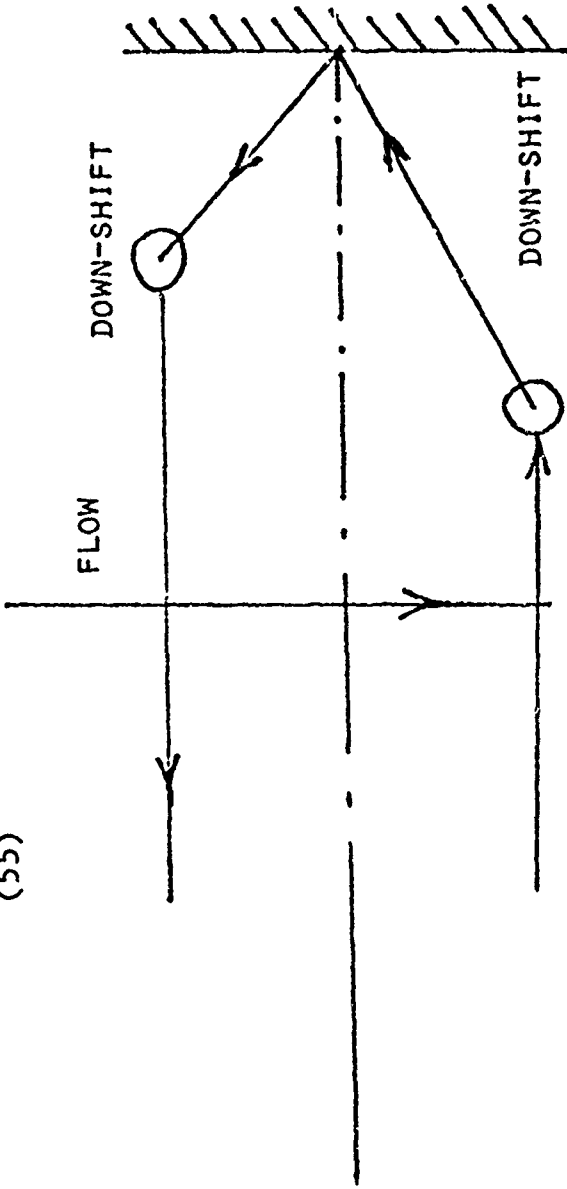


FIGURE 6

(56)

CORNER-CUBE REFLECTOR

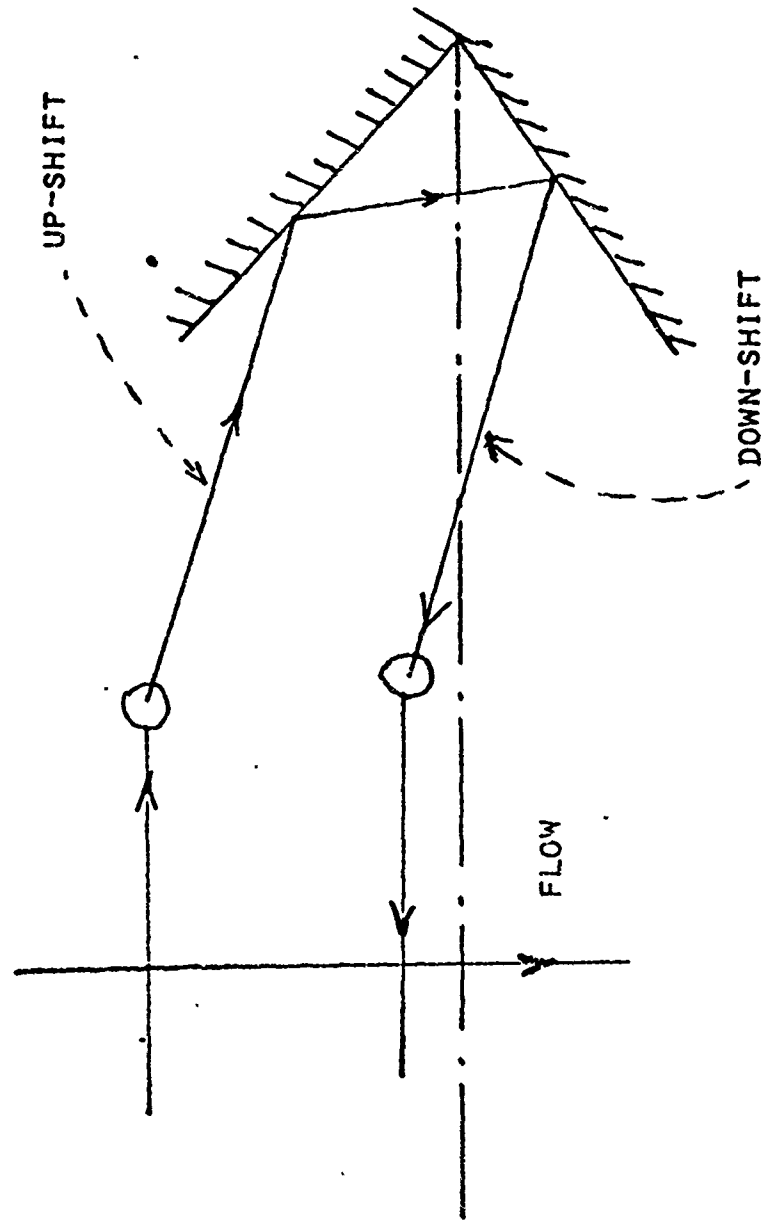
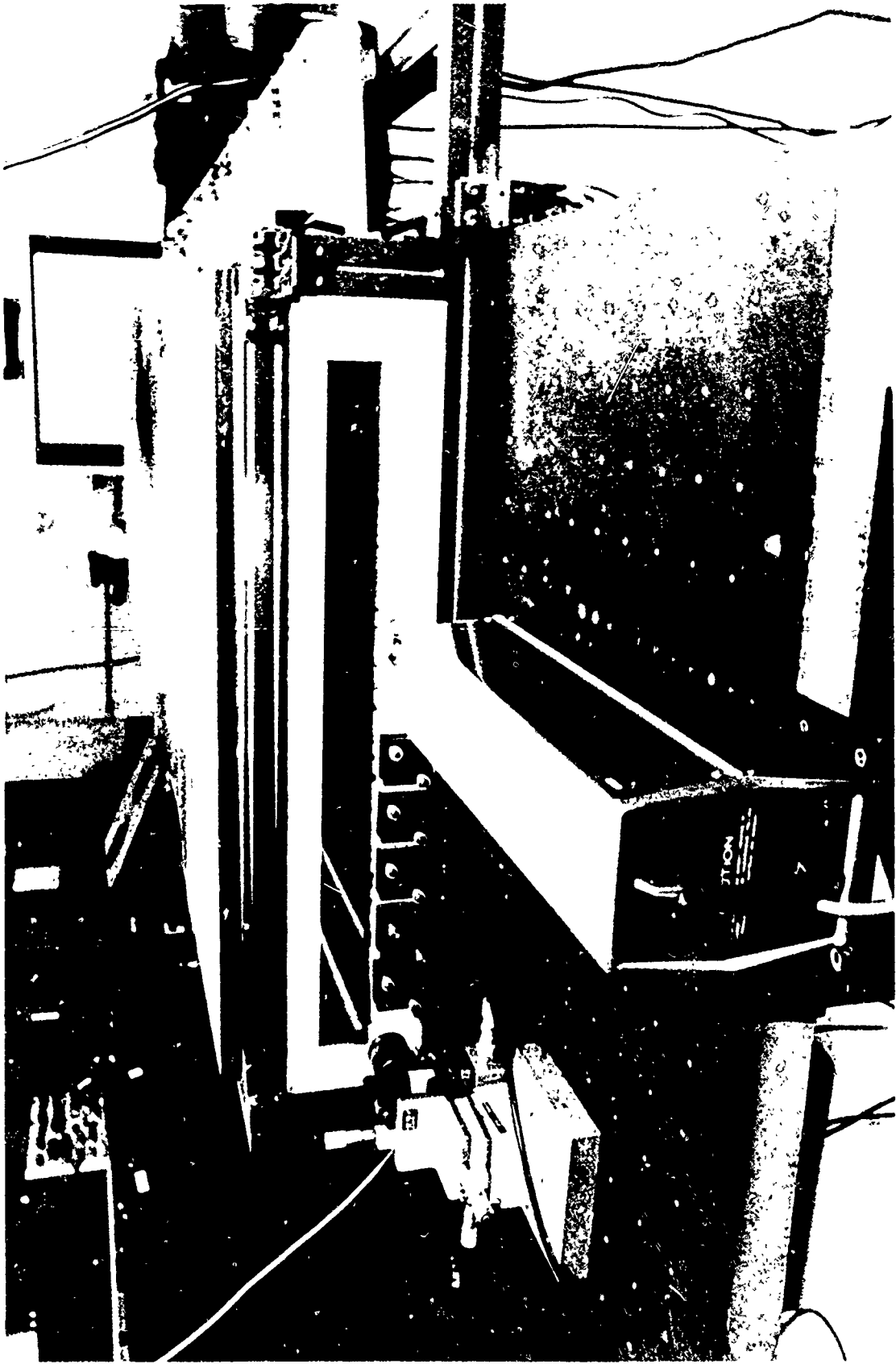
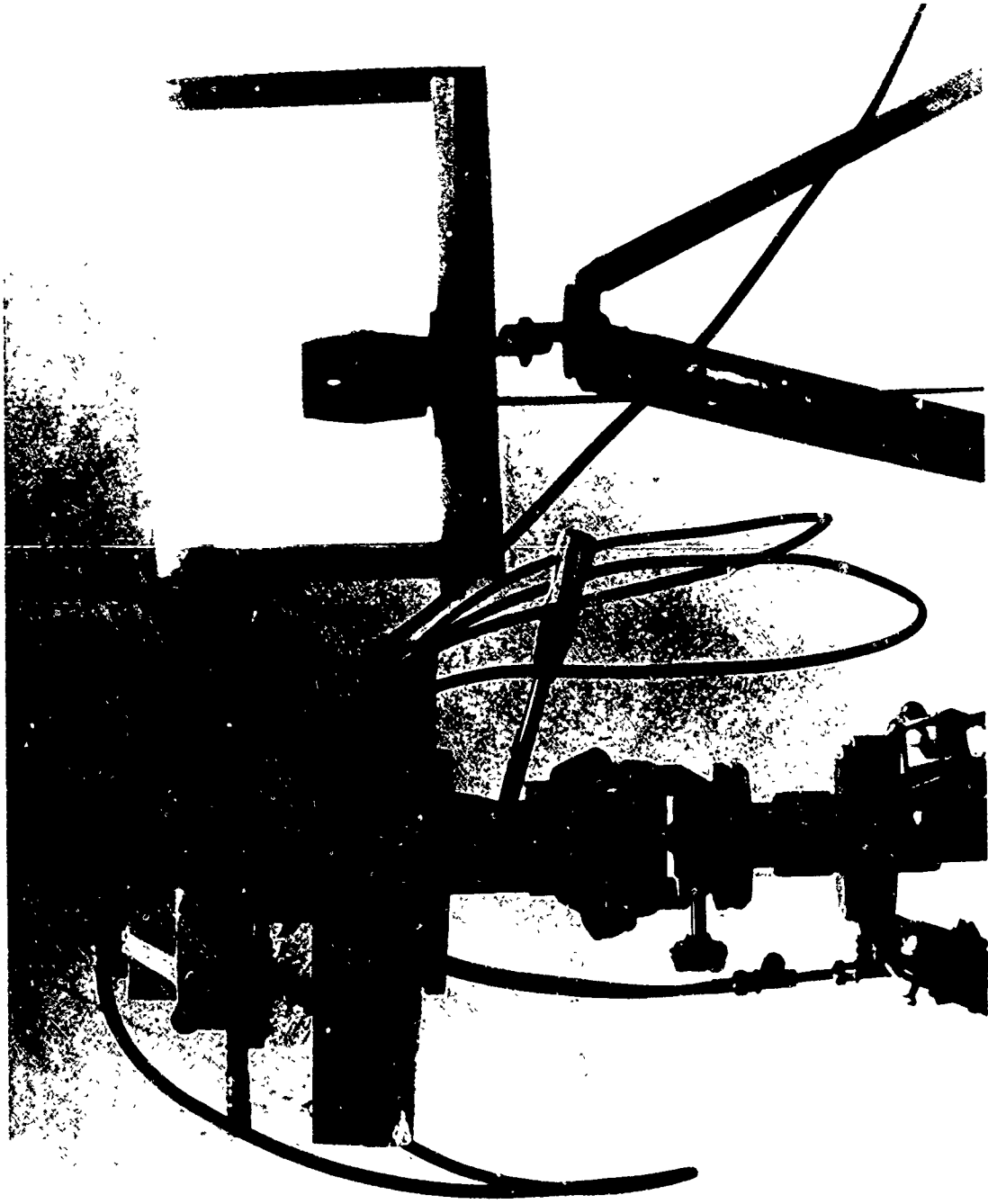


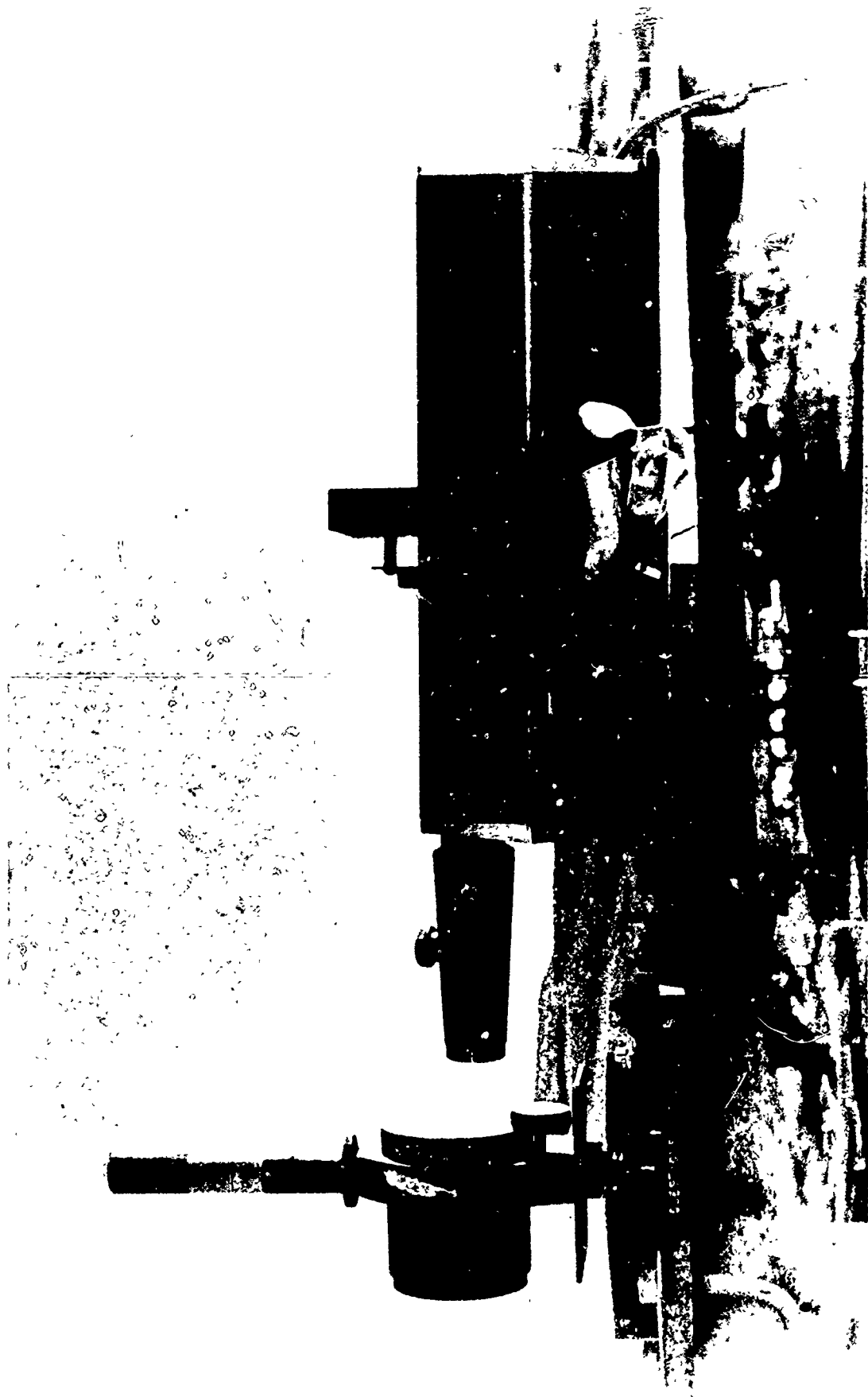
FIGURE 7



ATMOSPHERIC TURBULENCE CHAMBER
AND
MULTIPLE TRANSMISSION EXPERIMENT



A HE-NE LASER TRANSMITTER AND A RECEIVING TELESCOPE
WITH PHOTOMULTIPLIER



A CORNER CUBE AND FLAT MIRROR REFLECTORS AND
A HE-NE LASER FOR DIRECT TRANSMISSION EXPERIMENT